Comparison of delta and uniform doped p-type and n-type ZnO films

By

Ravichandra Reddy Gade

Submitted in Partial Fulfillment of the Requirements

for the Degree of

Master of Science

in the

Electrical Engineering

Program

YOUNGSTOWN STATE UNIVERSITY

August, 2015

Comparison of delta and uniform doped p-type and n-type ZnO films

Ravichandra Reddy Gade

I hereby release this thesis to the public. I understand that this thesis will be made available from the OhioLINK ETD Center and the Maag Library Circulation Desk for public access. I also authorize the University or other individuals to make copies of this thesis as needed for scholarly research.

Signature:

____

Ravichandra Reddy Gade, Student Date

Approvals:

____

Dr. Tom Nelson Oder, Thesis Advisor Date

____

Dr. Jalal Jalali, Committee Member Date

____

Dr. Philip C. Munro, Committee Member Date

____

Dr. Salvatore A. Sanders, Dean of Graduate Studies Date

Abstract

ZnO is a wide band gap semiconductor with unique optical, electrical, magnetic and thermal properties. The major road block for the fabrication of ZnO based optoelectronic devices is the difficulty of achieving high and stable p-type conduction in ZnO. Highly conductive n-type ZnO materials are obtained easily with extrinsic dopants. Most of the p-type and n-type ZnO materials reported in literature were produced by the standard procedure of uniform doping. In the literature, delta doping technique has enhanced p-type conduction in wide band semiconductors like GaN, AlGaN and ZnSe as compared to uniform doping method. There are few reports about delta doped n-type ZnO materials. The goal of this study is to obtain reliable and highly p-type conductive ZnO through delta doping and to investigate the difference of p-type and n-type conductivities in delta and uniform doped p-type and n-type ZnO films.

The properties of p-type and n-type ZnO thin films doped with acceptors (lithium and phosphorous) and donor (aluminum) have been characterized. All the films were prepared on sapphire substrates by rf (radio frequency) magnetron sputtering. Uniform doping of the films was accomplished by simultaneous sputtering from ZnO and Li_3PO_4 targets for p-type doping and from ZnO and Al targets for n-type doping. For delta doping, the deposition from Li_3PO_4 or Al targets was interrupted periodically. Hall effect measurements on O_2 annealed p-type films revealed p-type conductivities with an average Hall concentration of 3.76×10^{13} cm^{-3} in uniform doped film and 1.3×10^{16} cm^{-3} in delta doped films. The as-grown delta doped n-type film exhibited an average Hall concentration of 2.79×10^{19} cm^{-3} whereas uniform doped n-type film showed an average concentration of 1.82×10^{18} cm^{-3}. The electrical conductivity in n-type films was

enhanced upon annealing in ($N_2 + O_2$) gas ambient. X-ray diffraction scans indicated that the crystal quality of delta and uniform doped p-type and n-type films improved significantly after annealing. The low temperature (12 K) photoluminescence (PL) scan results revealed the presence of more defects in uniform doped n-type films than in delta doped n-type films. The PL scan on p-type films showed an acceptor-related luminescence peak at 3.35 eV which is due to the transition from exciton bound to a neutral acceptor.

Acknowledgements

Foremost, I would like to express my sincere gratitude to my advisor **Dr. Tom Nelson Oder** for the continuous support of my research. I appreciate his vast knowledge and skill in many areas and his assistance in writing my thesis report. I could not have imagined having a better advisor for my Master's thesis. I will forever be thankful.

My special thanks to the National Science Foundation for supporting this work through grant (DMR#1006083).

I thank my committee members Dr. Jalal Jalali and Dr. Philip C. Munro for their support and guidelines. I would also like to thank Youngstown state University for giving me an opportunity to work in the Department of Physics & Astronomy as research assistant.

Assistances by Dr. Matthias Zeller (for XRD measurements) and Dr. Dingqiang Li (for EDS measurements) from the Department of Chemistry are also gratefully acknowledged.

Finally I would like to extend deepest gratitude to my parents for their love and encouragement. I thank all the members who directly or indirectly helped me to complete my research work.

Table of Contents

Abstract iii

Acknowledgement v

List of Figures ix

List of Tables xii

Abbreviations xii

Chapter 1 Characteristics of ZnO 1

1.1 Introduction 2

1.2 Crystal structure and electrical properties 3

1.3 Transparency 4

1.4 Luminescence properties 5

1.5 Summary of current processing techniques 6

1.6 Advantages 7

1.7 Applications 8

Chapter 2 Doping in ZnO 10

2.1 Doping 10

2.1.1 p-type doping and its difficulty 10

2.1.1.1 Group V acceptors 11

2.1.1.2 Group I acceptors 12

2.1.2 n-type doping 13

2.2 Monodoping and codoping 14
2.3 Uniform doping 15
2.4 Delta (δ) doping 16
2.4.1 Historical review 19
2.4.2 Merits of delta doping over uniform doping reported in literature 20
Chapter 3 Experimental techniques 22
3.1 Sputtering 22
3.1.1 Principle of sputtering 23
3.1.2 Magnetron sputtering 24
3.1.3 Influence of vacuum pressure on sputtering 26
3.1.4 Comparison of RF and DC magnetron sputtering 27
3.2 Deposition chamber 27
3.2.1 Vacuum system 29
3.2.2 Target and sputtering gun assembly 29
3.2.3 Substrate preparation and loading 30
3.2.4 Temperature controller and thermocouple 31
3.2.5 Vent valve and mass flow controller 31
3.2.6 RF power 31
3.2.7 DC power 32
3.2.8 Thermistor gauge and ion gauge 32

3.2.9 Shutter....32

3.3 Photoluminescence (PL) spectroscopy....33

3.3.1 Free exciton transition....35

3.3.2 Bound exciton complexes....35

3.3.3 Donor-acceptor transition complexes....35

3.3.4 Free to bound transition....36

3.3.5 Experimental set-up....37

3.4 Hall effect....39

3.5 Van der Pauw resistivity and Hall measurements....41

3.5.1 Resistivity measurement....42

3.5.2 Hall measurements....43

3.5.3 Ecopia Hall measurement system....45

3.6 Annealing....45

Chapter 4 Results and Discussion....48

4.1 Procedure for growing p-type and n-type ZnO films....48

4.2 Experiments conducted for p-type ZnO films through monodoping and results....49

4.3 Experiments performed for p-type ZnO through codoping....50

4.3.1 Sample Structures....51

4.3.2 Results and analysis....52

4.3.2.1 Energy-dispersive X-ray spectroscopy (EDX)....52

4.3.2.2 Photoluminescence (PL) scan 53

4.3.2.3 X-ray spectroscopy scan (XRD) 55

4.3.2.4 Hall effect measurements...56

4.4 Second set of experiments conducted for p-type ZnO through codoping 60

4.5 Experiments conducted for n-type ZnO through monodoping 61

4.6 Results and analysis 62

4.6.1 Hall results of as-grown n-type ZnO films 62

4.6.2 Hall results of N_2 and (N_2+ O_2) annealed n-type ZnO films 65

4.6.3 XRD scan..66

4.6.4 PL scan..68

Chapter 5 Conclusion...70

5.1 Conclusion 70

5.2 Future work 71

References..72

List of figures

Figure 1 Wurtzite structure of ZnO 2

Figure 2 PL spectrum of undoped ZnO 5

Figure 3 Applications of ZnO 9

Figure 4 Schematic of a semiconductor epitaxial film with δ-doping layer 17

Figure 5 Calculated sub-band energies and wave-functions of δ-doped GaAs 18

Figure 6 Diode sputtering system 23

Figure 7 Magnetron sputtering 25

Figure 8 Magnetron sputtering deposition chamber 28

Figure 9 Schematic sketch of magnetron sputtering deposition chamber 28

Figure 10 ZnO target 30

Figure 11 Single side polished sapphire mounted on substrate holder 30

Figure 12 Double side polished sapphire mounted on substrate holder 31

Figure 13 Magnetron control software window 33

Figure 14 Photoluminescence schematic 34

Figure 15 Photoluminescence equipment 37

Figure 16 Schematic of photoluminescence equipment 37

Figure 17 Principle of monochromator operation 38

Figure 18 Hall effect measurement setup for metal 40

Figure 19 Van der Pauw contact placement 41

Figure 20 Van der pauw resistance measurement configurations 42

Figure 21 Van der Pauw configuration for the calculation of Hall voltage V_H 43

Figure 22 Ecopia Hall measurement system 45

Figure 23 Rapid thermal processor 46

Figure 24 Structure of codoped samples prepared by delta doping 51

Figure 25 Structure of codoped sample prepared by uniform doping 51

Figure 26 EDX data of 110813 sample 52

Figure 27 EDX data of 110613 sample 52

Figure 28 EDX data of 120213 sample 53

Figure 29 PL data of delta and uniform doped samples annealed at 700 ^{o}C 54

Figure 30 PL data of delta and uniform doped samples annealed at 900 ^{o}C 54

Figure 31 XRD scan of annealed and un-annealed delta and uniform doped ZnO films
....55

Figure 32 Repeated Hall-effect measurements on the delta doped (110613) sample showing the variation of a) Carrier concentration b) Mobility and c) Resistivity 57

Figure 33 Repeated Hall-effect measurements on the delta-doped (110813) sample showing the variation of a) Carrier concentration b) Mobility and c) Resistivity............58

Figure 34 Repeated Hall-effect measurements on the as-grown delta-doped (120213) sample showing a) Carrier concentration b) Mobility and c) Resistivity 59

Figure 35 Repeated Hall-effect measurements on the as-grown delta-doped (100614) sample showing a) Carrier concentration b) Mobility and c) Resistivity 63

Figure 36 Repeated Hall-effect measurements on the as-grown delta-doped (100614) sample showing a) Carrier concentration b) Mobility and c) Resistivity 64

Figure 37 XRD scan of annealed (N_2+ O_2) and un-annealed delta doped sample (032215) …..67

Figure 38 XRD scan of annealed (N_2+ O_2) and un-annealed uniform doped sample (121214)...67

Figure 39 PL data of delta and uniform doped samples annealed in (N_2 + O_2) 68

Figure 40 PL data of second set delta and uniform doped samples annealed in (N_2 + O_2).. 68

List of tables

Table 1 Properties of wurtzite ZnO 3

Table 2 Minimum resistivity and maximum carrier concentration obtained for ZnO films doped with various impurities 14

Table 3 Experiments conducted for making of p-type ZnO through monodoping 49

Table 4 Hall results of monodoped p-type ZnO films 50

Table 5 Experiments conducted for making of p-type ZnO through codoping 50

Table 6 Average p-type concentration of delta and uniform doped samples annealed at 900 ^{O}C in O_2 60

Table 7 Second set of experiments conducted for making of p-type ZnO films 60

Table 8 List of experiments conducted for n-type ZnO 61

Table 9 Electrical properties of specific as-grown n-type films 62

Table 10 Electrical properties of specific N_2 annealed n-type films 65

Table 11 Electrical properties of ($N_2 + O_2$) annealed n-type films 66

Abbreviations

PL Photoluminescence

ITO Indium Tin Oxide

Zn_i Zinc Interstitial

V_O Oxygen Vacancy

A:B Element A is doped with element B

[Where A = ZnO and B= N or Al or P or As or Li_3PO_4]

V_{Zn} Zinc Vacancy

A^OX Acceptor bound to exciton

MBE Molecular Beam Epitaxy

SCCM Standard Cubic Centimeters per Minute

Chapter 1

Characteristics of ZnO

1.1 Introduction

Zinc oxide (ZnO) is a very versatile material and belongs to the II-VI group in the periodic table. It exists in nature as mineral zincite. Its wide band gap of 3.4 eV and a large exciton binding energy of 60 meV at room temperature make it a promising semiconductor material for blue and ultra violet optical devices [1]. The rediscovery of ZnO and its potential applications in the 1950s have made it to undergo an intensive research. Discovery of good piezoelectric properties of ZnO in the year 1960 have led to its first application in the electronics field as a thin layer for surface acoustic waves [2].

ZnO has wide range of applications such as solar cells, piezoelectric transducers, varistors and sensors [1]. In the 1960s, several research studies have been conducted on ZnO fundamental properties such as energy band gap, electron and hole effective masses, and electrical transport properties. In 1965 Au Schottky barrier was made with ZnO and LEDs were demonstrated in 1967 [2]. Up to 1970s doping of impurities into ZnO has been studied [2]. From the1980s, the interest in ZnO has been decreasing due to the difficulty of achieving stable and high p-type conduction in ZnO [3]. Without good p-type ZnO materials, device development using ZnO will be greatly hampered. All the issues regarding p-type conduction in ZnO have been discussed in detail in Chapter 2.

1.2 Crystal structure and electrical properties

The crystal structure of ZnO is normally a hexagonal wurtzite with lattice constants a=3.25 Å and c = 5.207 Å. The Zn atoms are tetrahedrally coordinated to four oxygen atoms, forms a polar symmetry along the hexagonal axis as shown in Figure 1.

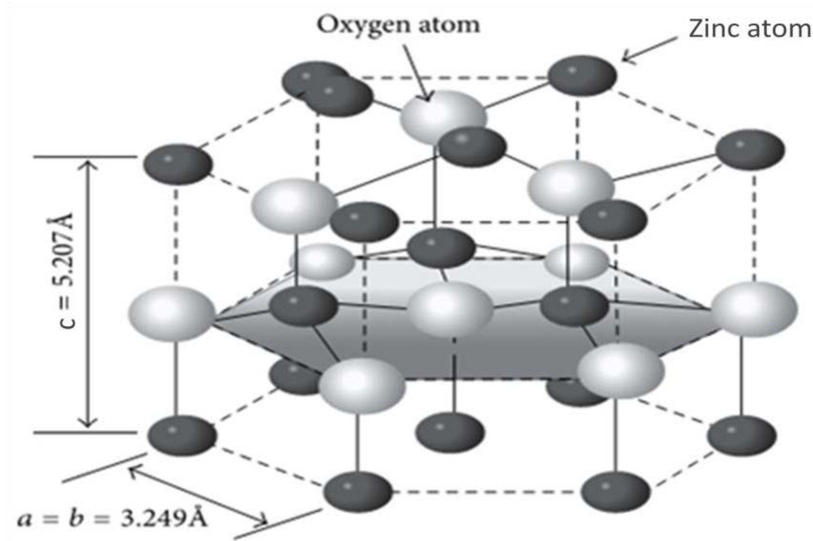

Figure 1 Wurtzite structure of ZnO [from ref 4].

The polar symmetry is a significant factor responsible for ZnO crystal growth, etching, defect generation and also many of its properties including piezo electricity and spontaneous polarization [1]. The nature of bonding in ZnO is strongly ionic (Zn^{+2} – O^{2-}) and this property makes it a good piezo electric material that has applications in signal processing, telecommunications and sensors. The basic properties of wurtzite ZnO are presented in Table 1.

Table 1 Properties of wurtzite ZnO [from ref 5].

Property	Value
Molecular formula	ZnO
Molar mass	81.4084 g/mol
Appearance	Amorphous white or yellowish white powder.
Hole mobility (at 300 K)	5-50 cm^2/V.sec
Density	5.606 g/cm^3
Melting point	1975 ^oC
Boiling point	2360 ^oC
Solubility in water	0.16 mg/100 mL
Refractive index	2.0041
Lattice constants	a_o = 0.32469 Å c_o = 0.52069 Å
Relative dielectric constant	8.66
Energy gap	3.4 eV
Intrinsic carrier concentration	$< 10^6$/cc
Exciton binding energy	60 meV
Electron effective mass	0.24 m_o
Electron mobility (at 300 K)	200 cm^2/V-sec
Hole effective mass	0.59 m_o

As-grown (undoped) ZnO is usually an n-type material. Initially this property was attributed to ZnO native defects such as oxygen vacancies (V_O) and zinc interstitials (Zn_i). Later it was realized through experiments and theory that oxygen vacancies are deep donors and zinc interstitials are unstable at room temperature, so they don't contribute for a considerable amount of n-type conductivity in ZnO [6].

Through first principal calculations Janotti and Van de walle showed that hydrogen atoms can fill the substitutional O sites and behave like shallow donors, which are responsible for the significant n-type conductivity in as-grown ZnO [7]. This statement holds true because hydrogen is present in all the growth methods and can diffuse easily into ZnO because of its high mobility [8]. The current carried in a doped ZnO can be a hole or electron current, which is determined by the dopants that account for the electrical properties in ZnO. The highest n-type conductivity achieved was 10^{21} electrons cm^{-3} [8] and largest reported p-type conductivity was 10^{19} holes cm^{-3}, but such high levels of p-type doping are questionable and have not been experimentally verified [1]. A detailed explanation of p-type and n-type conductivity in ZnO is given in the Chapter 2.

1.3 Transparency

ZnO is transparent to visible light and belongs to the group of the transparent conductive oxides (TCOs), which also includes indium tin oxide (ITO) and tin oxide. Due to high conductivity and high transparency (transmittance > 85%), TCOs can be used as transparent electrodes for liquid crystal displays (LCDs), organic light-emitting

diodes (OLEDs) and photovoltaic solar cells. ZnO dominates other TCOs in terms of low cost, higher conductivity (in case of tin oxide) and ease of etching (ITO) [9].

ZnO is drawing attention as replacement for ITO in LCDs because of the low cost of Zn metal and high cost, scarcity of indium. A research has been carried out to replace the opaque amorphous silicon (a-Si) in active matrix liquid crystal displays (AMLCDs) and AMOLEDs backplanes with ZnO based transparent thin-film select transistors (TTFTs). The study revealed that ZnO TTFTs has several advantages over conventional a-Si TFTs namely reduction of the gate voltage and higher channel mobility, device stability, on-to-off ratio > 10^6, transparency, low cost and low temperature processing [9]. The progress of transparent electronics depends upon the quality and processing of both n- and p- type materials.

1.4 Luminescence properties

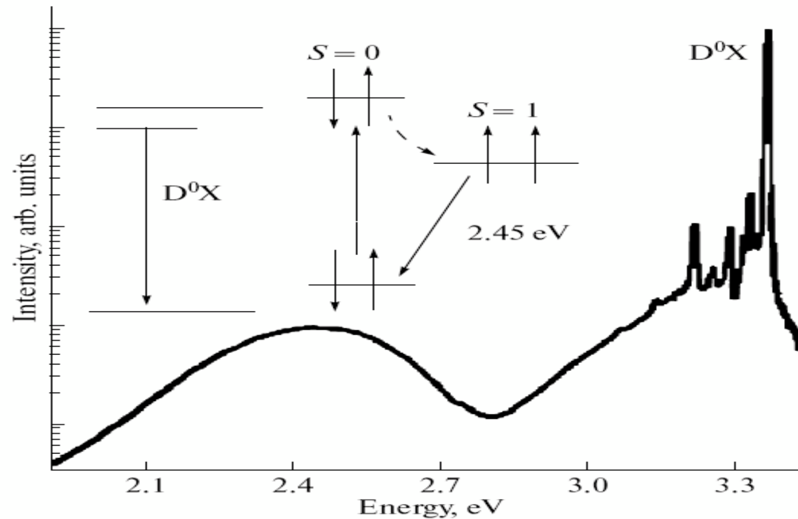

Figure 2 PL spectrum of undoped ZnO [from ref 10].

The sharp band edge luminescence peak at 3.36 eV is attributed to emission from the neutral donor bound exciton ($D^{O}X$) transition. The origin of donor responsible for this transition is still in debate.

The broad emission peak below 2.7 eV is the green luminescence band. Through optically detected magnetic resonance technique (ODMR), it was found out that neutral oxygen vacancy (V_O) in the undoped ZnO was responsible for the green band emission. In the ODMR experiment the undoped ZnO was exposed to light. This led to the transistion of two electrons of oxygen vacancy from ground state to an excited singlet state s=0 and relax at triplet state s=1. This resulted in the emission of green luminescence band which has maximun intensity at a peak value of 2.45 eV and is shown in Figure 2 [10].

1.5 Summary of current processing techniques

The epitaxial growth techniques of ZnO thin films have been studied with an interest in its potential applications such as acoustical and optical devices. The ZnO thin films are grown on different substrates in addition to glass, sapphire and diamond because of its strong (001) orientation with the substrate surfaces. Most of the epitaxial growth of ZnO is carried out on sapphire, which has advantages of low cost and availability in bulk quantities [8].

Advanced growth techniques used for the ZnO epitaxial growth are:

1. Radio frequency sputtering (RF Sputtering)
2. Molecular beam epitaxy (MBE)
3. Chemical vapor deposition (CVD)

4. Pulse laser deposition (PLD)

5. Physical vapor transport (PVT)

6. Vapor phase transport (VPT)

The advantages of RF sputtering and MBE include the delivery of high quality ZnO thin films and a control over the growth of ZnO epitaxial layers. CVD is a standard technique used by the industries for the production of high quality ZnO thin films. PVT method was initially used for the bulk growth of ZnO thin films and is currently used for epitaxial growth. VPT is an economical technique used for the fabrication of superior quality ZnO nanostructures and bulk crystals on a large scale [11]. PLD and MBE can be used for the deposition of good quality ZnO thin films at lower growth temperatures than GaN. This leads to the fabrication of electronic devices at low cost.

The above mentioned advanced epitaxial growth techniques occasionally give room for unintentional impurities during the growth of ZnO. The impurities also include deep level defects which may arise due to native ZnO defects or contamination of growth environment. These defects also create deep energy levels within the forbidden band gap of ZnO and act as trap centers for the carriers in the material [12]. This results in the deterioration of ZnO electrical properties. The widely used growth techniques are MBE, PLD and RF sputtering.

1.6 Advantages

In today's world, GaN is one of the most extensively used material for the applications of high power, high frequency, blue lasers and UV-LED devices. ZnO has several advantages over GaN, which makes it possible to consider ZnO as a replacement

for GaN in order to have a much better performance in the current electronic devices. The advantages are explained as follows.

ZnO has better radiation resistance than GaN. This makes it a suitable material for space and nuclear applications [1]. Its saturation velocity of $3x10^7$ cm/s is much larger than GaN, This enables the fabrication of fast electronic and optoelectronic devices. ZnO exciton binding energy (60 meV) is much larger than that of GaN (25meV), this should result in the production of UV sources with higher brightness and low power thresholds at room temperature [13]. Its very high break down electric field of $2x10^6$ V/cm is about two times higher than that of GaN and makes it more favorable to operate ZnO based devices at higher voltages and powers.

1.7 Applications

ZnO is an attractive material for gas sensors, piezo-electronic devices and transparent high power electronics [1]. ZnO nano size biosensors have been used to detect different biological molecules. ZnO based gas sensors have a potential ability of detecting gas molecules like NO_2, NH_3, NH_4, CO, H_2, H_2O, O_3 and C_2H_5OH. ZnO has been used successfully in thin film piezoelectric devices like bulk acoustic wave, surface acoustic wave (SAW) resonators, filters, sensors and micro mechanical systems. One of the most important potential application is the saw filter which is an important component in TV filters and wireless communication systems. ZnO based saw filters were used for UV photo detection, gas and biochemical sensing [14].

ZnO nano wires are attractive for the nano scale devices such as LED’s, laser’s, photo detectors, chemical/biosensor and saw devices because of their interesting

properties like good charge carrier transport and high crystalline quality. In comparison with GaN, The growth of ZnO large crystals can be achieved relatively easily. It is less toxic and has a lower impact on the environment [14]. ZnO serves as a dietary supplement in animal food and it can be used in many materials like facial powders, ointments, sunscreens, catalysts, lubricant additives, paint pigmentation, rubber and batteries [1]. Figure 3 shows the applications of ZnO in various fields.

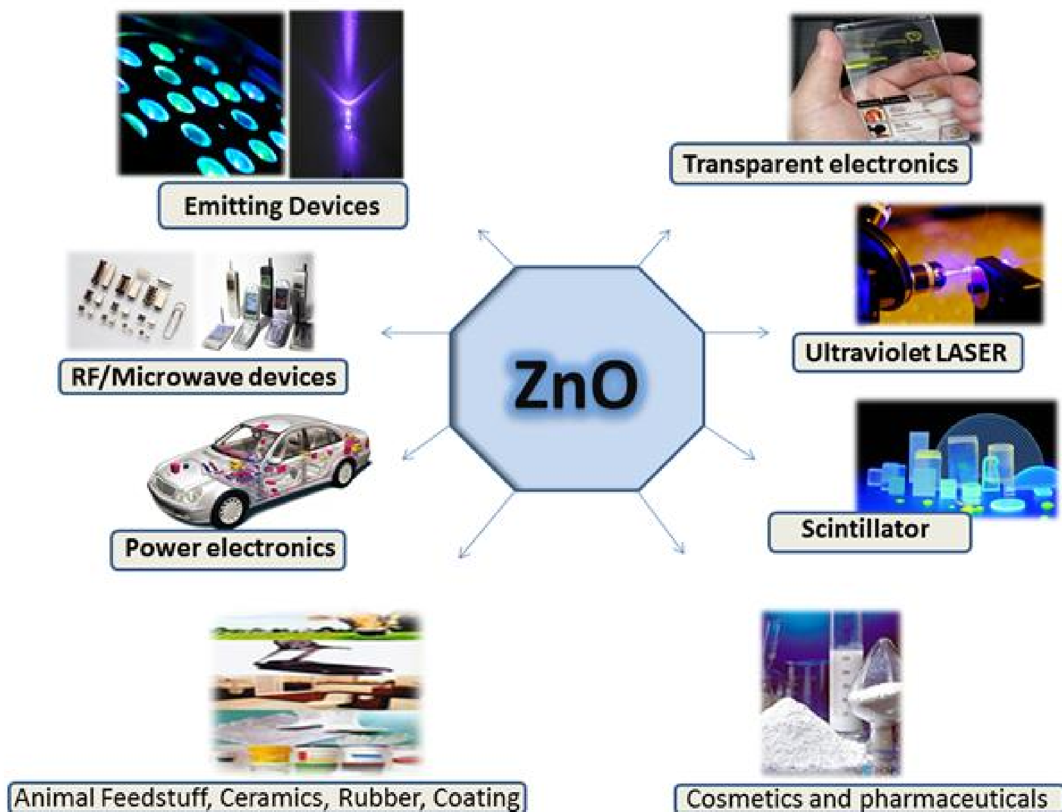

Figure 3 Applications of ZnO [from ref 15].

Chapter 2

Doping in ZnO

2.1 Doping

The process of adding other material to the crystal of intrinsic semiconductors to improve its conductivity is called doping. Wide band gap semiconductors exhibit strong preference for one type of doping for example ZnO, GaN, CdS, ZnS and ZnSe can be doped easily to n-type, while p-type doping is a problem and they have their valence band far from the energetic position of the vacuum level. P-type doping in ZnTe, CdTe and diamond is achieved easily and n-type doping is difficult [8].

Dopants in semiconductors are classified into two types based on their energy levels. Deep dopants are those which occupy the energy levels far from either conduction or valence band and require very high thermal energy to get ionized whereas shallow dopants need less energy to get ionized. The detailed analysis of doping in ZnO is carried out in sections 2.1.1 and 2.1.2.

2.1.1 p-type doping and its difficulty

Lack of high quality p-type ZnO material is a major road block to its development. The main reason for this is the unstable behavior of p-type conductivity in ZnO which could be due to the compensation of its p-type dopants by low energy native defects, such as Zn_i or V_O or H impurities [8].

There have been many reports about switching of conductivity (p-type to n-type) in p-type ZnO films within a matter of days. Apart from compensation problems, it was proposed that the low solubility of p-type dopants in ZnO and precipitate formation were also the possible causes for the unstable conductivity in p-type ZnO films [8]. Group V and group I elements are the p-type dopants in ZnO and their role in ZnO is explained as follows.

2.1.1.1 Group-V acceptors

Among the group V elements, nitrogen is the most promising acceptor for producing p-type ZnO because its ionic radii (1.68 Å) is close to oxygen ionic radii (1.38 Å) as compared to arsenic (2.22 Å) phosphorous (2.12 Å) and antimony (2.45 Å). However, recent experimental investigations have shown that N_O is a deep acceptor in ZnO with a large ionization energy of 1.3 eV [16]. Nitrogen acceptors may get compensated by defects such as O-vacancies, complexes with Zinc interstitials or N_2 molecules [17].

Through first principal pseudo-potential calculations Lee et al. [18, 20] found out four possible compensation mechanisms for nitrogen acceptor in ZnO using N_2 as N source. They were (a) N-acceptor-Zn-antisite complex (b) N_2 molecule at an O site (c) split-interstitial-O_i complex (d) N-acceptor-Zn-interstitial complex. It was shown that the N acceptors were mainly compensated by oxygen vacancies at low N concentrations, while at high concentrations of N, N-acceptor-Zn-antisite complexes were the major compensating defects. There are many reports of unstable p-type conductivity in nitrogen doped ZnO films for example ZnO: N films grown on glass through sputtering showed p-

type conductivity, which reverted to n-type after repeated measurements in the dark and returned back to p-type only after exposure to light.

First principle calculations predicted that substitutional P at an O site is a deep acceptor because of its large ionic radius as compared to O and has high ionization energy of 0.62 eV. This makes it impossible to achieve efficient p-type doping in ZnO with P_O. Under zinc rich growth conditions, dominant donors like P_{Zn} compensate the Po acceptors leading to n-type conduction in ZnO. The first-principle pseudo potential calculations revealed that p-type ZnO can be achieved in O-rich growth conditions and V_{Zn} defects are the favorable acceptors in phosphorous doped ZnO films grown using P_2O_5 source, while P_{Zn}-$2V_{Zn}$ complex account for p-type conductivity in ZnO films fabricated using Zn_3P_2 source [19].

Arsenic has large mismatch of ionic radii of As^{3-} with O^{2-} and most of the As atoms stay on the Zn site. This makes arsenic as ineffective acceptor in ZnO. However, with the analysis of PL spectrum data of As doped ZnO grown on GaAs, it was predicted that the $As_{Zn} – 2V_{Zn}$ complexes are shallow acceptors in p-type ZnO: As films and have ionization energy of 0.15eV [20]. Based on the first principles computations, it was proposed that $Sb_{Zn} – 2V_{Zn}$ complexes are shallow acceptors and are responsible for p-type conductivity in ZnO: Sb films [21].

2.1.1.2 Group-I acceptors

First principal calculations showed that the Group-I impurities such as Li and Na are shallow acceptors in ZnO. The calculated ionization energies by Park et al. were 0.09eV for substitutional Li_{Zn}, 0.17eV for Na_{Zn} and 0.3eV for K_{Zn} [22].

Electron paramagnetic resonance (EPR) measurements showed that Li_{Zn} atoms cause a serious relaxation among the neighboring O atoms. The exposure of ZnO: Li films to light at low temperatures causes the excitation of hole, which gets trapped on some of the oxygen atoms along the C axis and has energy lower than the non-axial sites [17]. Li_i and Na_i act as electron donors and compensate the Li_{Zn} and Na_{Zn} acceptors to a large extent. Thus Li and Na interstitial impurities should be eliminated in order to achieve a reliable p-type ZnO.

2.1.2 n-type doping

n-type doped ZnO films are the most promising transparent conductive oxides (TCOs) to be used as transparent electrodes in different applications. ZnO can be doped n-type easily compared to p-type doping. The n-type dopants that can be used are group III elements Al, Ga and In, group IV elements Si, Ge and Sn, group VII elements Cl and F that can substitute for oxygen and rare earth metals Sc and Y. Group III elements are the preferred substitutional elements for Zn because of their low vapor pressures as compared with group VII elements [8]. Table 2 shows minimum resistivity and maximum carrier concentration obtained (from literature [8]) for ZnO films doped with various impurities

As the bond length of In-O (2.1 Å) is greater than the Zn-O (1.97 Å), indium causes a serious deformation of the ZnO lattice as compared to Al and Ga and currently-ZnO:Al and ZnO:Ga films are the best substitutes for ITO in the thin film transparent electrode technology. Both the films have high transmittance in the visible region and

large electrical conductivity values. This is why Al and Ga are considered to be promising candidates for n-type doping in ZnO.

Table 2 Minimum resistivity and maximum carrier concentration obtained for ZnO films doped with various impurities [from ref 8].

Dopant	**Dopant content (Wt %)**	**Resistivity (x10^{-4} Ω-cm)**	**Carrier Concentration (x 10^{20} cm^{-3})**
Al_2O_3	1-2	0.85	15.4
Ga_2O_3	2-7	1.2	14.5
B_2O_3	2	2.0	5.4
Sc_2O_3	2	3.1	6.7
SiO_2	6	4.8	8.8
V_2O_5	0.5-3	5.0	4.9
F	0.5	4.0	5.0

2.2 Monodoping and codoping

Monodoping involves doping of ZnO with one dopant impurity, which may be an acceptor or donor. According to the literature [8], monodoping with n-type impurities such as Al and Ga have produced highly conductive n-type ZnO films, while achievement of good p-type materials through monodoping of acceptors into ZnO is a major challenge. This is due to the acceptors compensation problems that are discussed in detail in section 2.1.1. These problems have directed the focus of research on the usage of non conventional methods such as codoping.

Yamato [23] proposed codoping with donor and acceptor impurities would increase the acceptor solubility and reduces the acceptor binding energy, thus leads to the production of highly doped p-material. There have been few reports on codoping with two acceptor elements. Through first principle calculations Tian and Zhao [24] predicted that co-doping with N and P would lead to the formation of acceptor P_{Zn}-$4N_O$ complexes, which have lower formation energy than P_{Zn} under Zn rich condition may result in the enhanced p-type conductivity in ZnO. Lu et al. [25] obtained stable p-type ZnO by co-doping with Li and N and it was proposed that the complex acceptors such as Li_{Zn}-N_O and Li_{Zn}-N eliminated the donor compensating defects such as Li_i.

In this study, codoping has been implemented on ZnO with lithium and phosphorous for the achievement of good p-type material and monodoping of ZnO with Al has been carried out for n-type material. All the other details relating to codoping and monodoping in p-type and n-type ZnO films are given in Chapter 4. Codoping and monodoping were realized using two methods namely a) uniform doping and b) delta doping which are explained as follows.

2.3 Uniform doping

It is a common method used to dope the semiconductors by using one of the epitaxial growth techniques. The dopant atoms are distributed throughout the semiconductor film during its growth. The interaction of dopants with the semiconductor defects is more likely in uniform doping than in delta doping. This leads to the self compensation of dopant atoms, consequent drop of carrier concentration and increase of

resistivity in uniform doped semiconductor films. This change will have serious effect on the material electrical and optical properties.

2.4 Delta (δ) doping

Delta doping in epitaxial grown semiconductors leads to a narrow doping profile thereby increasing the dopant concentration which will be an advantage for many device applications. The achievement of narrow doping profile is possible only if doping atoms are bound to a single atomic layer of host semiconductor as shown in Figure 4, which shows a semiconductor substrate and dopant sheet sandwiched between the epitaxial layers [26].

Delta doping bounds all the doping atoms to a single atomic layer in the host semiconductor. The position of dopant sheet and density of dopant atoms in the sheet are the two important factors in deciding the properties of a delta doping profile. Wafer surface is assumed to be in the x-y plane of a Cartesian coordinate system and z-coordinate is measured from surface to bulk. The plane $Z=Z_d$ consists of dopant atoms and the resulting doping profile is given by the formulae

$$N(Z) = N^{2D}\,\delta(Z-Z_d) \quad \ldots\ldots (1)$$

where the two-dimensional (2D) density, denoted by N^{2D} is the number of doping atoms in the doping plane per cm^2. Equation (1) states that the doping concentration is zero for all locations, except for $Z = Z_d$ [26].

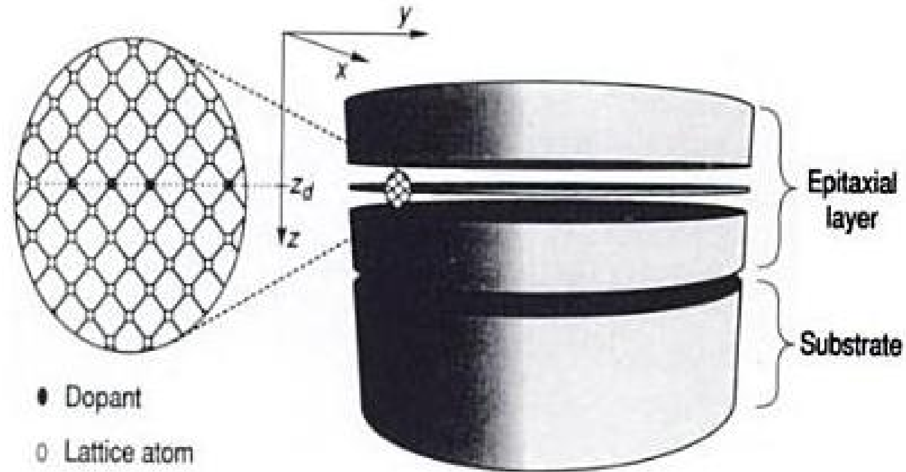

Figure 4 Schematic of a semiconductor epitaxial film with δ-doping layer [from ref 26].

The 2D doping density is obtained by integrating the equation (a) given by

$$\int_{-\infty}^{\infty} N(z)dz = N^{2D} \quad \text{...} \quad (2)$$

The dopant distribution given by the equation 1 results in a potential well whose energy is

$$E\,(Z) = \begin{cases} -\dfrac{eN_D^{2D}(Z - Z_d)}{2\in} \text{ for } z \le z_d \\ +\dfrac{eN_D^{2D}(Z - Z_d)}{2\in} \text{ for } z \ge z_d \end{cases} \quad \text{........................} \quad (3)$$

where elementary charge e = 1.6 x 10^{-19} coulombs. The equation (3) means that the potential well is V- shaped and symmetric with respect to Z_d.

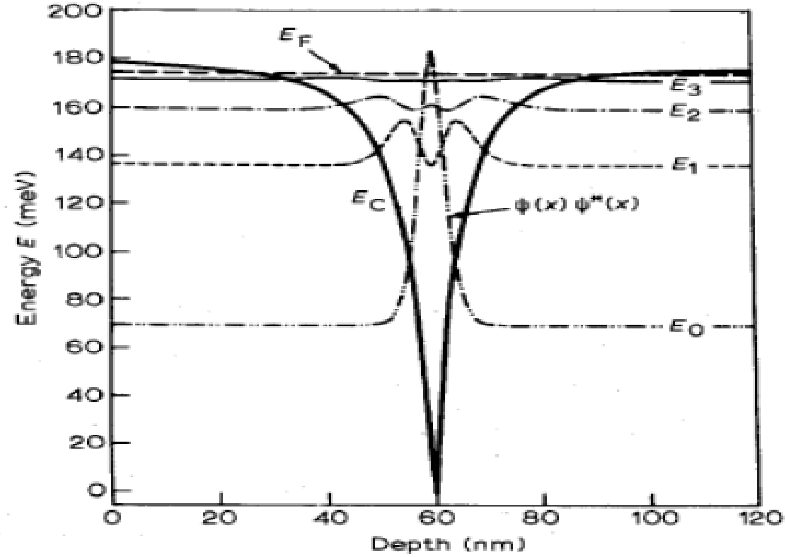

Figure 5 Calculated sub-band energies and wave-functions of δ-doped GaAs [from ref-27].

The Figure 5 is an example for V-shaped potential well, which was formed in δ-doped n-type GaAs. If the width of potential well is comparable to debrogile wavelength, it results in the quantization of allowed electron energies as shown in the figure and its four sub-band energies were calculated from a self consistent solution of the Poisson's and Schrodinger equations for GaAs with a sheet donor concentration of $5x10^{-12}$ cm^{-2}. Due to the presence of sub-energy bands, there would be enhancement in the carrier concentration of δ-doped planes as compared to uniform doped slabs.

The common method of delta doping for any growth technique is [26]

1) The growth of host semiconductor on a substrate is allowed and growth of dopant atoms is blocked for a predetermined time.

2) The host semiconductor growth is suspended and substrate is exposed to dopant atoms for a set time and after that growth of dopant atoms is again blocked, while growth of the host semiconductor is resumed.

The ideal conditions for a narrow delta doping profile are as follows [26]

1) It should be assumed that substrate surface is atomically flat with no atomic terrace steps.

2) Desired sticking probability of dopant atoms on the host semiconductor should be one for a good solubility.

3) Substrate-epilayer interface should be free from impurities.

4) All the dopant atoms should exactly confine to one atomic plane.

5) Atoms should not be incorporated on wrong sites or associated with defects.

6) There should not be diffusion of impurities away from the plane.

2.4.1 Historical review

The first use of delta doping was reported by Bass in 1979. He used vapor phase epitaxy (VPE) to grow a dopant spike in the silicon doped GaAs film and the full-width at half maximum of the spike was greater than 200Å [26]. In 1980 Wood et al. [28] reported strong adsorption of silicon on GaAs substrate surface that is synthesized by molecular beam epitaxy (MBE). The resulting dopant profile width was greater than 300Å. The first truly δ-doped semiconductor structure with clear evidence for narrow doping profile was reported by Schubert et al. (1984) and Schubert and Ploog (1985) [26, 29]. The MBE grown GaAs sample exhibited a full profile width of 40Å, which was at least five times narrower than the profile widths reported by Bass (1979) and Wood et al. (1980) [28]. The first field effect transistor fabricated using δ-doped GaAs was reported

by Schubert and Ploog in 1985 [29]. The δ-doped FET has a narrow free-carrier and dopant distribution and large gate-breakdown voltage.

Schubert and his coworkers manufactured a number of semiconductor devices with δ-doping technique using MBE included homojunction FET, the high mobility hetrojunction FET and lasers. The δ-doping technique in heterojunction FET'S yielded the highest free carrier concentration. In modulation-doped FET'S, the technique delivered optimum doping profiles. δ-doping in Led's and lasers has been used in the active region of their structures in order to activate the electron-hole recombination. The δ-doping in N-type $Al_XGa_{1-X}S$ samples have reduced the persistent photoconductivity (PPC) and free-carrier freeze-out, these two defects play a key role in the deterioration of properties in many semiconductor devices including microwave transistors [26]. Today δ-doped samples are characterized by using many methods such as secondary ion mass spectroscopy (SIMS), capacitance-voltage (CV) methods, tunneling, magneto-transport measurements, luminescence, Raman scattering and infrared absorption. In summary δ-doping applications have included a number of novel (or) improved device structures-[27].

2.4.2 Merits of delta doping over uniform doping reported in literature

Nakarmi et al. [30] obtained enhanced p-type conduction in a delta doped GaN: Mg film with a fivefold reduction in resistivity as compared to uniform doped GaN and also there was reduction in the dislocation densities and self compensation of Mg impurities. δ-doping silicon in the barrier region of AlGaN/GaN HFET Structures improved their dc performance and break down voltage over those of uniform doped ones

[30]. Bayram et al. employed delta doping for Mg doped p-type GaN and achieved a double order magnitude of higher doping with a fourfold reduction in resistivity and a decrease of activation energy over uniform doped materials [31].

Contreas et al. observed reduction of threading screw dislocations in GaN, which is delta doped with Si using MOCVD [32]. Chen at al. [33] achieved 92% increase in the hole concentration and 12% improvement of Mg doping efficiency in GaN using indium surfactant-assisted delta doping method. Jung et al. improved p-type doping in ZnSe by delta doping it with N and Te and created an interest among the II-VI wide band semiconductor group for the fabrication of blue-green lasers [34-35].

It was proposed that delta doping technique can reduce the complex-type compensating defects and increase the p-type doping level in II-VI wide-band-semiconductors in which achieving p-type doping is a big challenge [30].

Chapter 3

Experimental techniques

In this chapter, the basic concepts pertaining to different kinds of sputtering are explained along with the design of sputtering deposition chamber. All the p- and n-type ZnO films analyzed in this study were fabricated in this chamber. The optical properties of the films were determined with the photoluminescence equipment. The details of the setup are introduced. Finally the description about Hall Effect measurements and annealing are presented.

3.1 Sputtering

Sputtering is a process of dislodging atoms from a solid target surface by bombarding it with high energetic particles in a plasma. The solid target surface can be a metal or insulator or an oxide material. The energetic particles hitting the target surface can be atoms, ions, electrons, photons, neutrons, molecules and molecular ions such as $[N_2]^+$, $[O_2]^+$ and Ar^+. The sputtering process takes place in a closed glass chamber that will have a high vacuum pressure. Sputtering is like a sort of atomistic sand blasting. If the knocked out atoms deposit on a nearby substrate i.e. the material to be coated then the process is called sputter deposition [36].

Sputter deposition is used for the film deposition on semiconductor wafers, on magnetic media and head surfaces, for coating tools, for reflective coatings on window glass, for coating the insides of plastic bags and the surface of automobile parts, and a number of other wide applications [36].

3.1.1 Principle of sputtering

Sputtering is a type of physical vapor deposition, which uses the principle of momentum transfer to knock out the atoms from the target surface. A simple schematic of diode sputtering system is shown in Figure 6. The material to be sputtered (target) is loaded on the cathode and connected to a negative power supply which could be either DC OR RF. The substrate is placed on the anode and it can be heated, cooled, biased or could be a combination of these. This setup is placed inside a vacuum chamber filled with inert gas Ar through sputtering gas inlet [37].

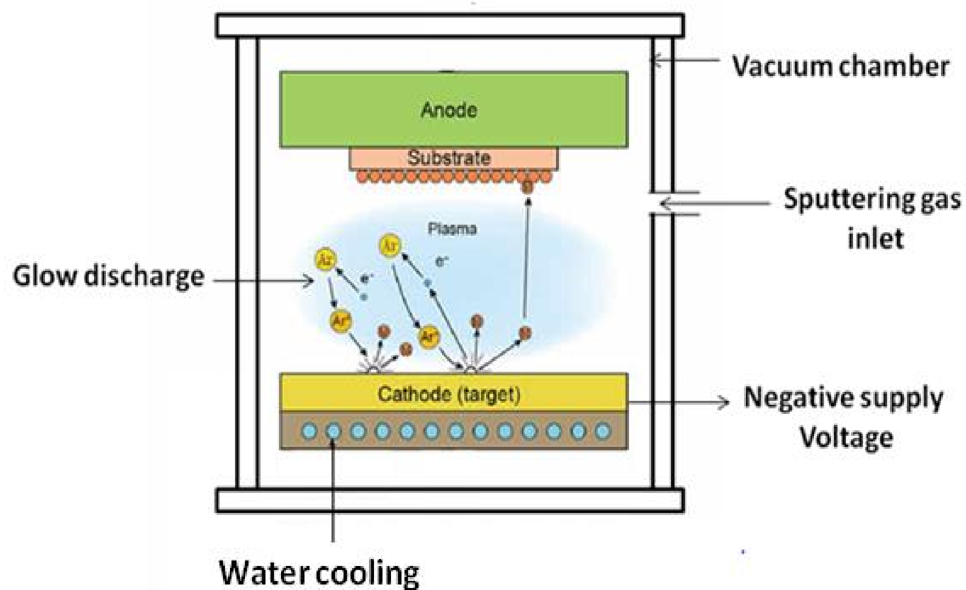

Figure 6 Diode sputtering system [adapted from ref 38].

On the application of high negative voltage to the target surface, it emits electrons, which collide with Ar atoms to cause ionization and excitation. Ionization leads to the creation of Ar^+ ions and secondary electrons, while the excitation leads to the glow discharge plasma. The Ar^+ ions get accelerated towards the negatively charged target

surface and bombard it with a transfer of net kinetic energy from the ions to the target atoms. By this, the atoms of the target material are ejected by the momentum transfer. The sputtered neutral atoms get deposited on the substrate. The secondary electrons repeat the process of ionization and excitation for a continuous sputtering deposition. The water cooling system prevents the overheating of the target, which is due to the usage of high sputtering power.

The sputter yield is just the ratio of the number of emitted particles (atoms) per incident particle (ion), given by

$$Y = \alpha \frac{M + m}{(M + m)^2} \frac{E_m}{U_M} \quad \text{...} \quad (4)$$

where Y= number of emitted particles/number of incident particles and M is the mass of the target atom, m is the mass of bombarding ion, E_m is the Kinetic energy of bombarding ion, U_M is the bonding energy of the target material. The parameter α depends upon the angle of ions bombarding the target surface [39]. The major problems with diode sputtering are the slow deposition rates and requirement of high voltage and current inputs.

3.1.2 Magnetron sputtering

The problem of slow deposition rates in the diode sputtering technique was solved by a powerful deposition technique called magnetron sputtering. It is the current work-horse of sputter deposition field, used in perhaps 95% of all sputtering applications [36].

A magnetron sputtering cathode uses magnets behind the target to create a closed static magnetic field configuration above it as shown in Figure 7. This confines the motion of secondary electrons near to the target surface to sustain the plasma. The secondary electrons above the target get trapped by the magnetic field and move in a direction perpendicular to electric and magnetic fields direction.

The secondary electrons in the magnetic field loose their kinetic energy due to collision with the sputtering Ar gas atoms resulting in an extremely dense plasma in the the magnetic field rings and ions created in it have high probablity of colliding the cathode surface, which eventually results in the improvement of ionization efficiency by several orders of magnitude.

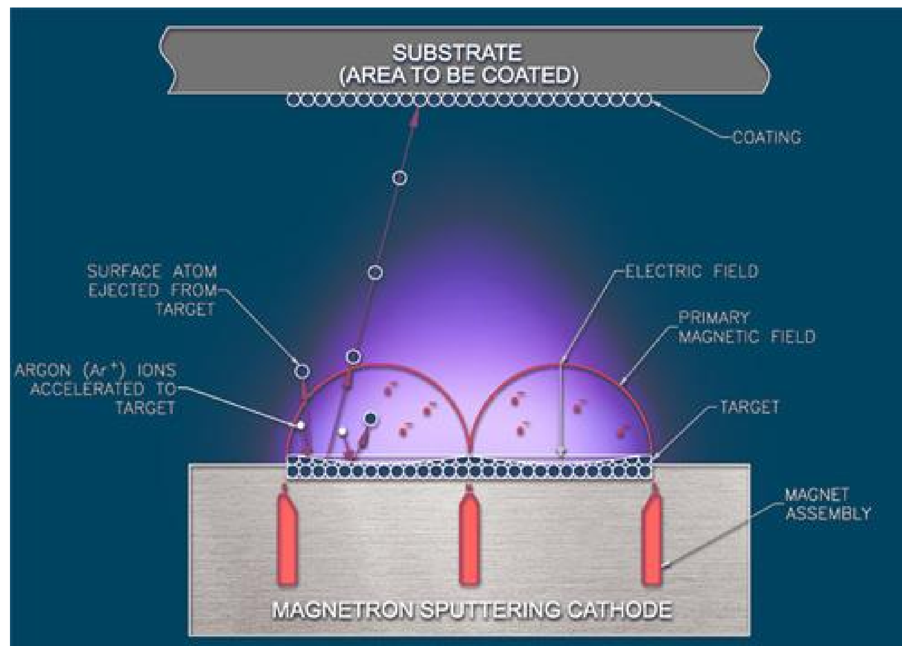

Figure 7 Magnetron sputtering [from ref 40].

The magnetron sputtering uses a lower gas pressure to maintain high sputtering rate and reduces the electron bombardment on the substrate. This leads to the growth of a thick film on the substrate with high purity. The sputtering rate is given by the equation

$$R = \frac{62.3 * J * Y * M_t}{\rho} \text{ Å/min} \quad \ldots\ldots (5)$$

where J is the ion current density, Y is the sputtering yield, M_t is the atomic mass of target material and ρ is the density. The above equation implies that sputtering rate depends upon on all the parameters in it [41].

3.1.3 Influence of vacuum pressure on sputtering

In the case of high vacuum pressure, the mean free path of an atom in a sputtering ambient is $\lambda = 4.8\times10^{-3}$ /P (torr) (cm). E.g. $\lambda \sim 0.1$cm for P=50mTorr. This implies the separation between the target and substrate is many cm and sputtered atoms have to undergo hundreds of collisions before reaching the substrate. The deposition rate is significantly reduced and causes the material to be deposited on the chamber walls [42].

In the case of low vacuum pressure, the higher ion energy increases the sputtering yield. But there will be fewer argon ions to bombard the target surface, which will reduce the deposition rate. Therefore, there exists an optimum pressure for which the deposition rate and plasma glow is maximum [42]. The condition for the optimum plasma glow is given by

$$L * P = 0.5 \text{ (cm.torr)}$$ L: electrode spacing, P: vacuum pressure

3.1.4 Comparison of DC and RF magnetron sputtering

Direct current magnetron sputtering uses a direct voltage to power up the magnetron sputtering cathode and used to sputter metals but not insulators. Due to high resistivity of insulators, a high impossible DC voltage of 10^{12} Volts is required to pass current through them. The lack of current will extinguish the plasma and stop the process. Thus DC sputtering can be applied only for the materials with a resistivity less than 10^6 Ω-cm i.e. metals. The solution for the problem of sputtering insulators with DC voltage is the usage of RF sputtering or AC voltage because the impedance of the dielectrics vary with the frequency of the voltage so that the current will sustain through the insulator [43]. The power supply of RF magnetron sputtering is operated at a high frequency of 13.6 MHz and the advantage of this technique over DC sputtering is its ability to sputter both insulators and metals. However, RF sputtering is a complex system that needs a separate impedance matching network as an additional component that is why DC magnetron sputtering is used to deposit metals [37].

3.2 Deposition chamber

All the sputtering experiments involved in this study were done in the magnetron sputtering deposition chamber as shown in Figure 8. The system consists of a main cylindrical glass bell jar enclosed in a cylindrical steel cage of 18 inches in diameter and 28.5 inches in height. The other main units include vacuum system, three magnetron cathode electrodes, substrate holder, temperature controller and RF/DC power supply.

44].

Figure 8 Magnetron sputtering deposition chamber.

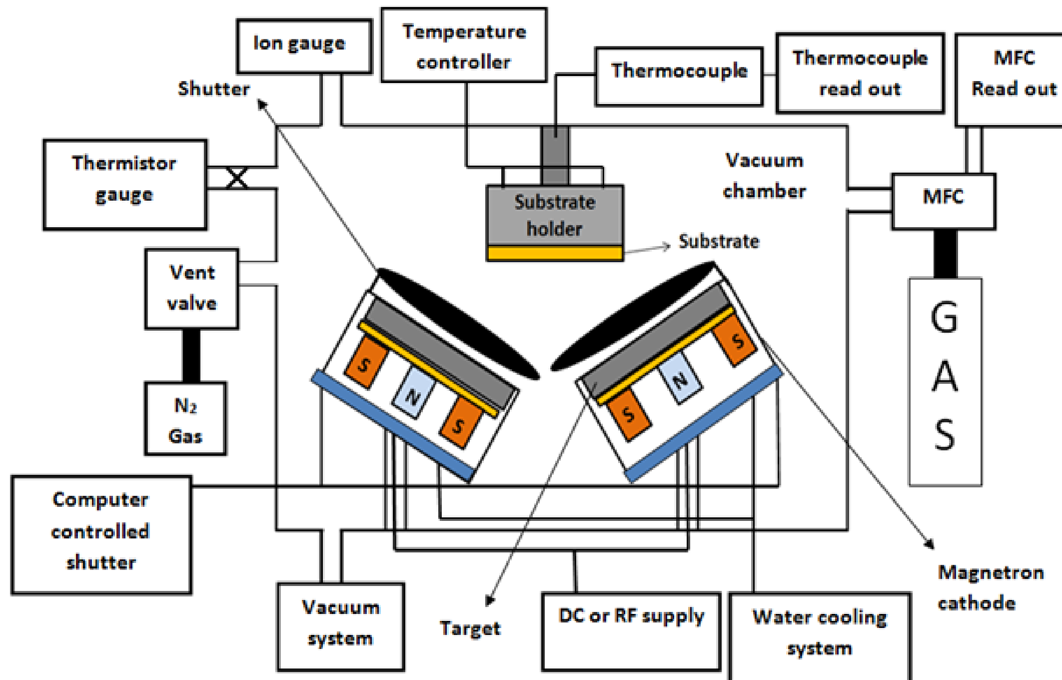

Figure 9 Schematic sketch of magnetron sputtering deposition chamber [adapted from ref 44].

All the units of magnetron sputtering deposition chamber are shown in its schematic Figure 9. The explanation to each unit is as follows.

3.2.1 Vacuum system

The vacuum inside the vacuum chamber is created and maintained by the vacuum system. The selection of vacuum system depends upon the factors like pumping rate and achievement of optimum low pressure. The vacuum system used for the deposition chamber is a combination of turbomolecular pump and mechanical pump, which can pump down the vacuum chamber to a low vacuum pressure of 10^{-7} mTorr.

3.2.2 Target and sputtering gun assembly

The targets used for the preparation of p-type and n-type ZnO thin films were 99.999% pure ZnO target along with the dopant targets such as Zn_3As_2, Zn_3P_2, ZnO/P_2O_5, Li_3PO_4, Al and Zno/Al (2% by weight). The ceramic targets are bonded to a copper plate to increase heat dissipation and preserve the target from cracking and all the targets are of same size of in diameter (2-inch) and thickness (0.125-inch). The Angstrom science magnetron cathode guns are used to sputter the targets and are designed to hold the 2-inch targets. One magnetron cathode gun is dedicated to the ZnO target and the other gun uses a target depending upon the material to be doped into ZnO. The water cooling system prevents the over heating of the targets during sputtering. The Figure 10 shows the ZnO target used for the experiments in this study.

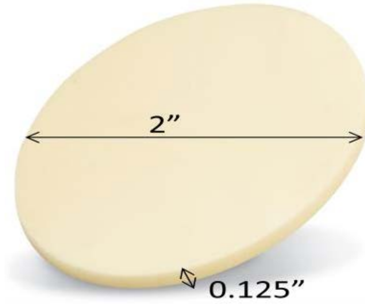

Figure 10 ZnO target [from ref 45].

3.2.3 Substrate preparation and loading

The substrates used for the preparation of p-type and n-type ZnO thin films were single-side polished and double-side polished C-plane sapphires which have a thickness of 430 μm and were cleaned using the standard RCA (Radio corporation of America) process, which was to boil in acetone (3 min), to boil in isopropyl alcohol (3 min) and to clean with de-ionized water. The substrates were then placed in diluted hydrofluoric acid ($1HF:10H_2O$) for three minutes, rinsed with de-ionized water and dried for a clean dust free surface. The substrates were then loaded on the substrate holder as shown in Figures 11 and 12.

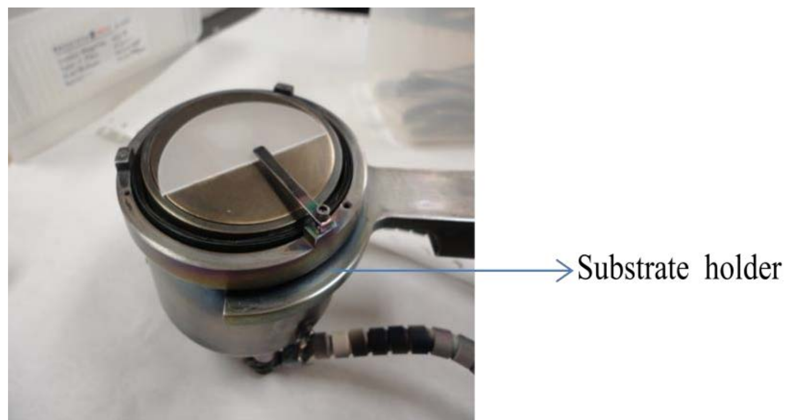

Figure 11 Single side polished sapphire mounted on substrate holder.

Figure 12 Double side polished sapphire mounted on substrate holder.

3.2.4 Temperature controller and thermocouple

The temperature controller can heat the substrate up to 900 ^{O}C and the thermocouple inserted into the substrate holder monitors the temperature of the substrate and displays it in the form of a digital reading through the thermocouple read out.

3.2.5 Vent valve and mass flow controller (MFC)

The purpose of vent valve is to get the chamber pressure from vacuum to atmospheric value through letting in pure N_2 gas into the chamber by opening the vent valve. MFC measures and controls the flow of sputtering gas inside the chamber and displays the gas flow value through MFC read out.

3.2.6 RF power

The RF power supplied for one magnetron cathode gun is provided using an external AJA 100/300 Seren industrial power source with Mc_2 automatic matching network control for RF tuning. The other gun uses RF VII INC source with PT-II-CE matching network. The power supplied to the guns controls the amount of atoms

sputtered from the target material by the sputtering gas ions. In this study, p-type and n-type ZnO films were fabricated on sapphire substrates by sputtering of ZnO and dopant targets with an RF power of 100 W.

3.2.7 DC power

Advanced energy MDX 500 was used as a source for the DC power supply. A direct current was used to power up the guns and to deposit ohmic contacts with gold and titanium targets on p- and n- type ZnO films for the purpose of Hall measurements.

3.2.8 Thermistor gauge and ion gauge

It is an instrument that constantly monitors and visually indicates the vacuum pressure of the vacuum chamber. It can measure the presuure only in a limited range of values (0 mTorr to 750 Torr). Below a pressure value of 0 mTorr, working of thermistor gauge is stopped automatically. This action leads to the activation of ion gauge equipment which there by can read the pressure values from 0 mtorr to 2×10^{-7} mTorr.

3.2.9 Shutter

The two shutters on the target materials (shown in Figure 9) have a back and forth movement controlled by a magnetron control software (designed in lab view) that is installed on computer. They were used to block and allow the deposition of target materials on the substrate at periodical intervals. The Figure 13 shows the magnetron control software window with shutter control parameters on it.

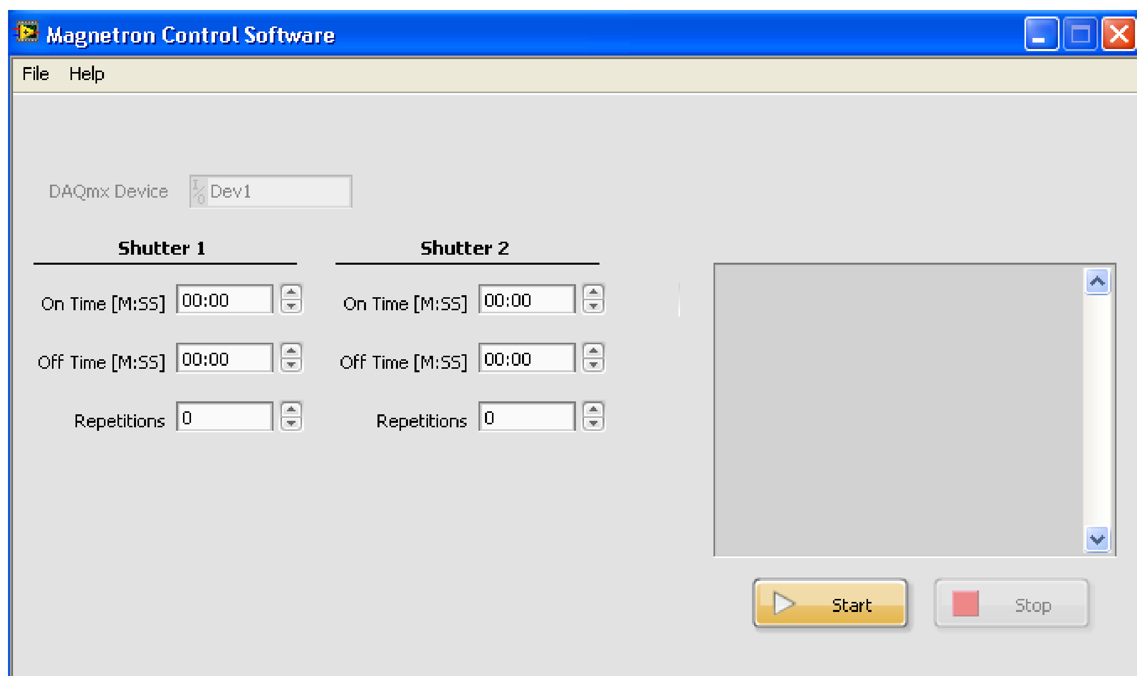

Figure 13 Magnetron control software window.

The on-time is the time for which the shutters will remain open and allow the deposition. In the off time, the shutter closes for a predetermined time and blocks the deposition. The on-time and off-time values are set depending upon how thick the p-type and n-type ZnO films are made. The shutter movement process can be repeated multiple times by setting a value in the repetition column.

3.3 Photoluminescence (PL) spectroscopy

Photoluminescence is a non-contact and non-destructive technique used for the analysis of optical properties of semiconductors, which include the determination of band gap energy (E_g), impurity levels and recombination mechanisms. PL involves the illumination of a high energetic monochromatic UV photon beam onto a semiconductor sample from a laser power source. The sample absorbs photons and electrons in it get

excited from valence band to conduction band (shown in Figure 14 (a)) leaving holes behind. In fraction of ns, the electrons get relaxed and fall into the valence band (shown in Figure 14 (b)) to recombine with holes The recombination of electron-hole pairs leads to the emission of luminescence (light) beam through the release of photons, which have energy equivalent to the band gap energy E_g and the recombination process is known as radiative recombination. The same is show in Figure 14 (c).

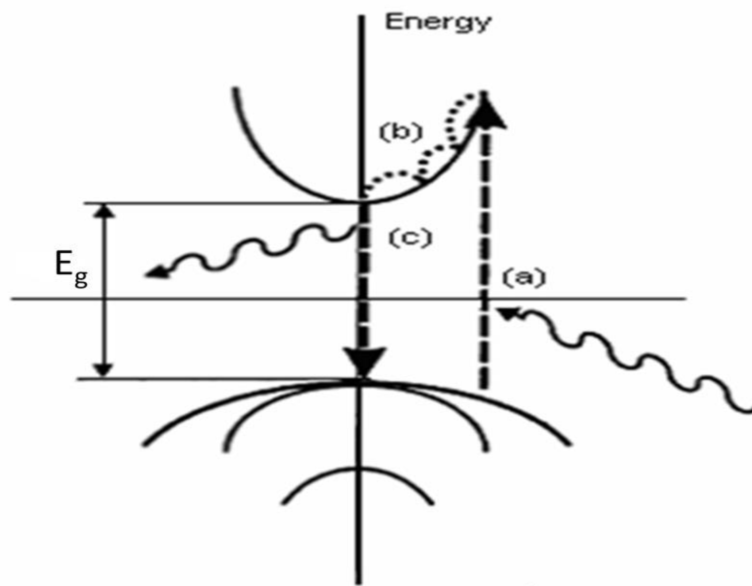

Figure 14 Photoluminescence schematic [from ref 46].

If the recombination leads to the emission of energy in the form of heat then it is called non radiative recombination. The whole mechanism of recombination process is also known as band to band transition. The impurities and defects in the sample also can emit photons through different types of radiative recombination events that are discussed as follows.

3.3.1 Free exciton transition

A free electron in the conduction band and a free hole in the valence band of a semiconductor get weakly bound together by a coulomb force to form a composite particle called exciton. It is like a hydrogen atom with electron orbiting the hole. If the exciton is not trapped by any defect or impurity then it is called free exciton. The energy of photon released in the excitonic recombination is given by:

$$h\nu = E_g - E_x \qquad (6)$$

where E_g is the band gap energy of the semiconductor and E_x is the coulomb energy of the exciton [47], h is the Planck's constant and ν is the frequency of emitted photon.

3.3.2 Bound exciton complexes

When a semiconductor at neutral state contains less number of donors or acceptors, the free excitons get captured by these impurities via Van der wall's interaction to form bound exciton complexes such as donor bound exciton ($D^{O}X$) and acceptor bound exciton ($A^{O}X$). Photons emitted due to the recombination of exciton bound complexes have the energy of

$$h\nu = E_g - E_x - E_b \qquad (7)$$

where E_b is the binding energy of the exciton to the impurity [47].

3.3.3 Donor-Acceptor pair transition

A donor and an acceptor in a semiconductor can get attracted by the coulomb potential to form a donor-acceptor pair (DAP) which move together in the semiconductor

crystal. The coulomb interaction increases as the distance between the donor and acceptor decreases. This action in turn will reduce the individual binding energies of donors and acceptors. The recombination energy of donor- acceptor pair is given by

$$E(r) = E_g - E_D - E_A + (e^2/4\pi \epsilon_o r) \quad (8)$$

where E_g is the band gap energy, E_D and E_A are the binding energies of the donor and the acceptor, $e^2/4\pi \epsilon_o$ is the coulomb interaction of the donor-acceptor pair separated by distance r [47].

3.3.4 Free to bound transition

The shallow impurities in a semiconductor get ionized at a temperature, where the thermal energy (K_B T) is greater than the ionization energy of impurities. K_B is the Boltzmann constant and T is the temperature. At very low temperatures, charge carriers in a semiconductor get trapped by the impurity which is due to the decrease of impurities thermal energy as compared to their ionization energy.

For example, in a p-type semiconductor that has N_A acceptors per unit volume, holes get trapped by the acceptors if the thermal energy is less than the ionization energy (E_A) of the acceptor. Free electrons can recombine radiatively with holes trapped on acceptors or holes can recombine with electrons trapped on donors resulting in free to bound transition. The emitted photon has energy of

$$h\nu = E_g - E_A \quad (9)$$

where E_A is the acceptor binding energy, the same equation can be written for the donor related free to bound transition by replacing E_A with E_D (donor binding energy) [46].

3.3.5 Experimental set-up

Figure 15 Photoluminescence equipment.

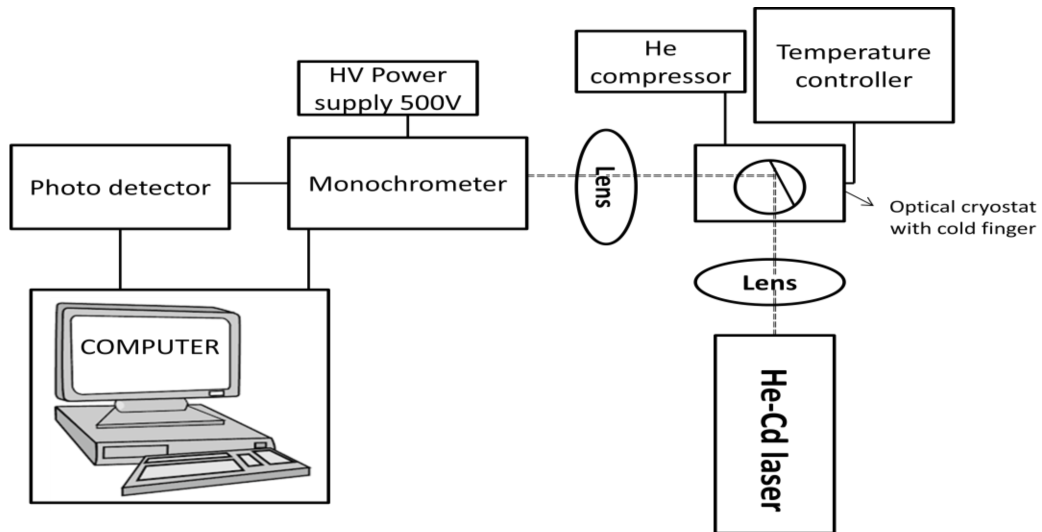

Figure 16 Schematic of photoluminescence equipment.

In this study the optical properties of p-type and n-type ZnO films were characterized using the Photoluminescence equipment shown in Figure 15. The Kimmon model no. IK3552R-G He-Cd laser (325 nm) is used as the optical excitation source in

the PL experiments. The samples were mounted on the cold finger at an angle of 45^0. The setup is placed into the Sumitomo model no. DF-202FF optical cryostat, which is cooled down from 300K to 12K with Sumitomo model no. HC-4E helium compressor for the purpose of taking low temperature PL measurements on the samples. The Cryocon model no. 32 temperature controller monitors the temperature of the samples. Once the temperature reaches to 12K the photoluminescence scan is started by the emission of UV beam from the laser as depicted in Figure 16. It is then passed through a lens and focused onto the film or sample surface, which absorbs the UV beam and emits the luminescence beam that gets collected at the lens and fed to the New Port model no. 6100 series monochromator, which is powered up using Tennecec Tc 952 500 V power supply.

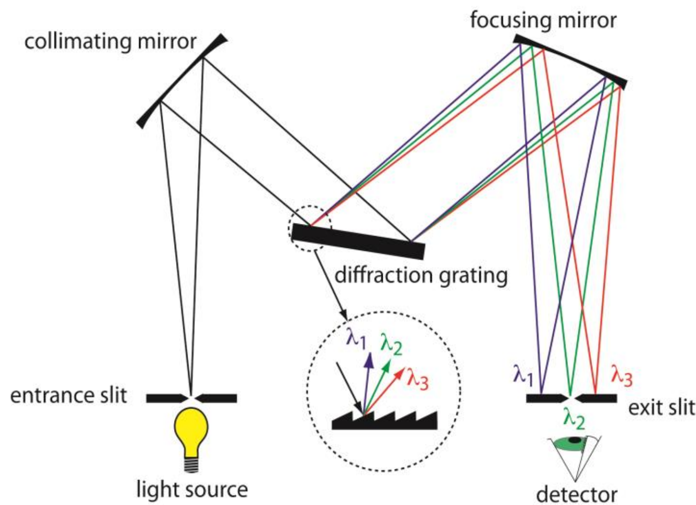

Figure 17 Principle of monochromator operation [from ref 48].

Figure 17 depicts the principle operation of the monochromator. The light beam coming from the entrance slit is reflected as beam of collimated rays by the collimating mirror onto the diffraction grating surface that has a series of etched ridges with a specific spacing and gets separated into individual colors having different wavelengths.

The focusing mirror collects the incoming light rays and reflects them at slightly different angles towards the different spots of the exit slit to form series of closely spaced individual color bands grouped by wavelength. The basic triac software installed in the computer tunes the monochromator to allow a particular wavelength of light to be passed from the exit slit to the photo detector which gets converted from optical signal to electrical signal. The computer takes the output electrical signal of photo detector and displays its amplitude reading.

3.4 Hall effect

If a specimen of metal or semiconductor carrying a current I is placed in a transverse magnetic field of flux density B then an electric field E is induced in the direction perpendicular to both I and B, which is known as Hall Effect. The Figure 18 shows the Hall Effect measurement setup for a metal. A voltage V_X is applied to the rectangular shaped metal bar so that current I flows in the positive X direction. The magnetic field is applied in the positive Z direction. At this condition the electrons inside the metal bar experience Lorenz force and get deflected towards the positive Y direction, thus creating Hall voltage V_H across the metal bar. The Lorenz force is given by

$$F = q\,(E + V \times B) \qquad (10)$$

Where $q = 1.6 \times 10^{-19}$ C and V is the electron velocity

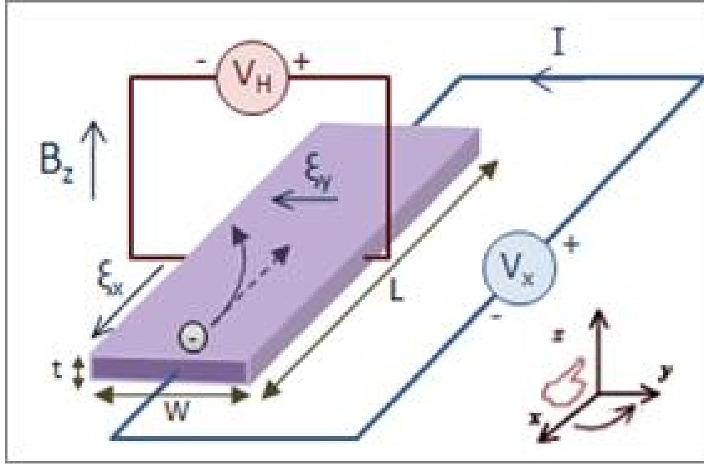

Figure 18 Hall effect measurement setup for a metal [from ref 49].

From the Lorentz force, the Hall coefficient R_H is calculated and defined as

$$R_H = E_y/J_x\, B_Z = -1/ne \quad (11)$$

where J is the current density of the electrons and E_y is the induced electric field

For semiconductor, Hall coefficient R_H is

$$R_H = \frac{p\mu_h^2 - n\mu_e^2}{e\,(P\mu_h + n\mu_e)^2} \quad (12)$$

where n is the electron concentration, p is the hole concentration, μ_h is hole mobility and μ_e is the electron mobility. From the value of R_H it is easy to determine carrier density and mobility.

3.5 Van der Pauw resistivity and Hall measurements

The disadvantage of the Hall Effect measurement is that it can be conducted only on samples that have Hall geometry as shown in Figure 18. Van der pauw technique can be used to measure resistivity, carrier density and mobility of any arbitrary shaped sample as long as it satisfies some conditions which are listed after Figure 19 [50].

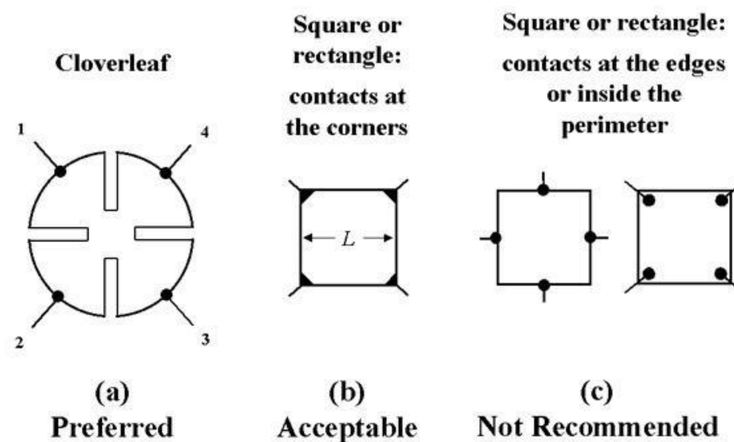

Figure 19 Van der Pauw contact placement

1. The four ohmic contacts on the sample should be located at the corners as shown by the picture a and b of Figure 19.
2. The contacts average diameter and sample thickness should be much smaller than the distance between the contacts as illustrated in Figure 19.
3. The sample should not have isolated holes and should be homogenous and isotropic.

3.5.1 Resistivity measurement

Figure 20 shows the Van der Pauw resistance measurement configurations. In this method four ohmic contacts are prepared at the four corners of the sample and four leads are connected to them. Two leads are used for passing the current to the sample and other two leads are used to measure the voltage across the contacts. The resistivity measurement starts with the application of positive DC current I_{14} to the contacts 1 and 4 and Hall voltage V_{23} is measured between the contacts 2 and 3. The Resistance $R_{14,23}$ is given by

$$R_{14,23} = V_{23}/I_{14} \ldots\ldots (13)$$

Similarly $R_{23,14}$ $R_{43,12}$ and $R_{12,43}$ are calculated by passing current and measuring voltage across desired contacts as shown in Figure 20 [50].

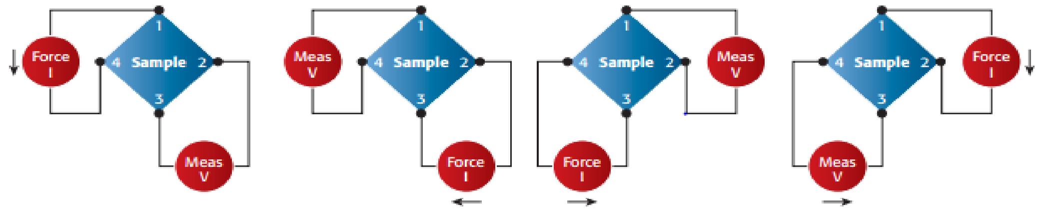

Figure 20 Van der Pauw resistance measurement configurations.

The sample resistivity (ρ) is calculated from the resistances R_A and R_B given by

$$R_A = (R_{21,34} + R_{12,43} + R_{43,12} + R_{34,21})/4 \ldots\ldots (14)$$

$$R_B = (R_{14,23} + R_{23,14} + R_{43,12} + R_{12,43})/4 \ldots\ldots (15)$$

$$\exp(-\pi R_A/R_S) + \exp(-\pi R_B/R_S) = 1 \ldots\ldots (16)$$

$\rho = R_S t$, t is the thickness of the sample.

3.5.2 Hall measurements

Calculation of Hall measurements for a semiconductor specimen through Van der Pauw method in magnetic field provides the values of sheet carrier density (n_s or p_s), bulk carrier density (n or p) and mobility of the specimen. For heavily doped samples the Hall voltage can be in the order of micro volts. The small voltage can have effect on the accuracy of Hall measurements when the sample shape is not uniform and contact placement is improper. These kinds of problems are eliminated by taking two sets of Hall measurements in positive and negative magnetic field directions [50].

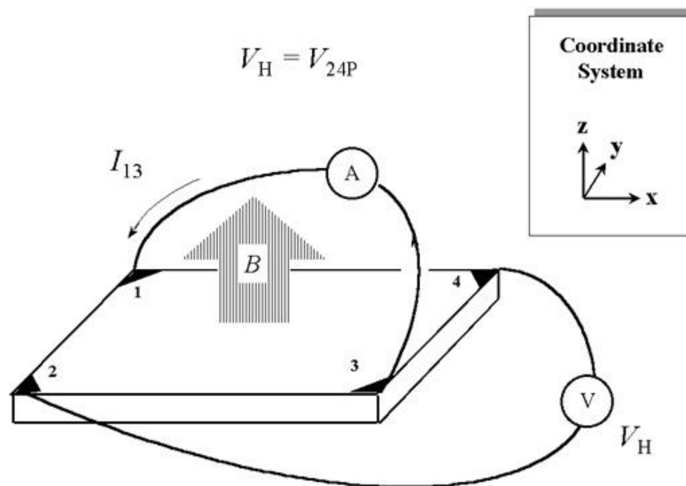

Figure 21 Van der Pauw configuration for the calculation of Hall voltage V_H

Positive magnetic field implies that B is applied in the positive Z direction and negative field is the application of B in the negative Z direction as shown in Figure 21.

The steps to be followed for taking the Hall measurement of any semiconductor sample are [50]

- Apply a positive magnetic field B.
- Apply a current I_{13} to contacts 1 and 3 and measure V_{24P} as shown in Figure 21.
- Apply a current I_{31} to contacts 3 and 1 and measure V_{42P}.
- Likewise, measure V_{13P} and V_{31P} with I_{42} and I_{24}, respectively.
- Reverse the magnetic field (negative B).
- Measure V_{24N}, V_{42N}, V_{13N}, and V_{31N} with I_{13}, I_{31}, I_{42}, and I_{24}, respectively.

The steps for calculating the carrier density and Hall mobility of the sample from the above voltages and currents are as follows

1. Calculate V_C V_D V_E V_F by using the following relations

   $V_C = V_{24P} - V_{24N}$, $V_D = V_{42P} - V_{42N}$, $V_E = V_{13P} - V_{13N}$, and $V_F = V_{31P} - V_{31N}$.

2. If $V_C + V_D + V_E + V_F$ is positive then the sample is p-type otherwise it is n-type.

3. The sheet carrier density (in units of cm^{-2}) is calculated from

   $p_s = 8 \text{ x } 10^{-8}\ IB/ [q\ (V_C + V_D + V_E + V_F)]$, if the voltage sum is positive

   $n_s = |8 \text{ x } 10^{-8}\ IB/ [q\ (V_C + V_D + V_E + V_F)]\ |$, if the voltage sum is negative

   where B is the magnetic field in gauss (G) and I is the dc current in amperes (A).

4. The bulk carrier density or carrier concentration (in units of cm^{-3}) is

$$N = n_s/t \text{ and } p = p_s/t \quad (17)$$

5. The Hall mobility $\mu = 1/qn_sR_S$ (in units of $cm^2V^{-1}s^{-1}$) is calculated from the sheet carrier density n_s (or p_s) and the sheet resistance R_S.

3.5.3 Ecopia Hall effect measurement System

The Hall measurements reported in this study were achieved using Ecopia HMS-3000 Hall Effect Measurement System shown in Figure 22.

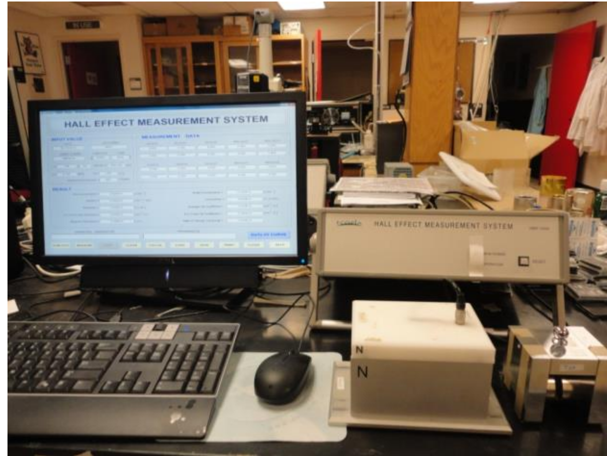

Figure 22 Ecopia Hall measurement System**.**

The system works on the principle of Van der Pauw geometry. It contains HMS-3000 software that checks the integrity of the sample ohmic contacts through Current-Voltage (I-V) measurements. The system can apply currents in the range of 1 nA to 20 mA and can measure carrier concentration from 10^{-7} cm^{-3} to 10^{-21} cm^{-3}. A permanent magnet of strength 1.05 T is used for the application of magnetic field. Once the HMS-3000 software is executed in the computer it automatically calculates the carrier concentration, mobility and resistivity of the sample.

3.6 Annealing

It is a process used in semiconductor device fabrication which consists of heating the samples at temperatures up to 1200 ^{O}C on a time scale of several seconds or less in a gas ambient.

The sample temperatures are then cooled down very slowly to prevent dislocations in their crystal structure. Annealing improves the crystal quality of doped materials by reducing the residual stress in them. It also activates the dopant atoms in the samples and increases their carrier concentration.

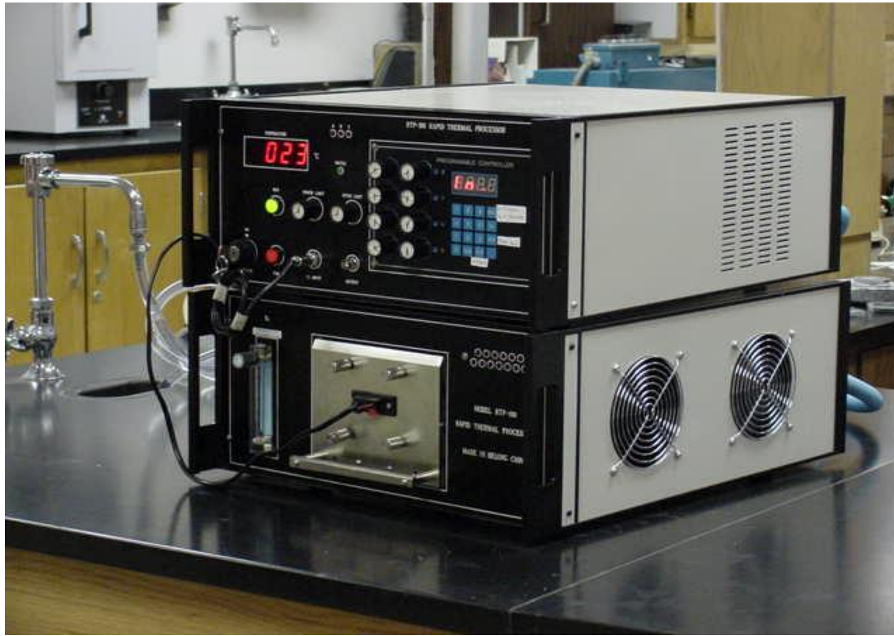

Figure 23 Rapid thermal processor.

In this work the RTP-300 rapid thermal processor shown in Figure 23 was used to anneal the p-type and n-type ZnO samples at temperatures 700-900 ^{O}C for 3-5 minutes using gases N_2 and O_2 to improve the electrical properties of the samples. The films to be processed were placed on the quartz tray, which goes into a quartz tube of the processor. Temperature and heating time were set with programmable controller and the desired gas pressure is controlled with the gas valve. The water cooling system is provided to prevent the processor from overheating. Once the annealing process is started the temperature is kept at constant value with the knobs of the controller. After annealing, the samples were

cooled down to room temperature and then the supply of gas and cooling system were shut off.

Chapter 4

Results and Discussion

This chapter deals with the results from experiments carried out on p-type and n-type ZnO films using uniform and delta doping techniques. The films were analyzed by photoluminescence (PL) spectroscopy, Hall-effect measurements and x-ray diffraction (XRD) spectroscopy. The p-type films were additionally investigated with the energy-dispersive X-ray spectroscopy and all the results are interpreted.

4.1 Procedure for growing p-type and n- type ZnO films

The c-plane sapphire substrates used in this study were cleaned according to the RCA cleaning process mentioned in Section 3.2.3. The substrates were then loaded into the vacuum chamber which was pumped to a base pressure of 2 x 10^{-7} Torr. The substrates were heated at 700 ^{O}C for 30 min in O_2 at 10 mTorr optimum pressure for a smoother substrate surface which was previously determined to be beneficial for achieving good quality ZnO films [51]. A 700 nm thick ZnO buffer layer was deposited on the substrate at 700 ^{O}C by sputtering the ZnO target with RF power of 100 W. A 1:1 mixture of ultrahigh-purity (UHP) Ar and O_2 at a pressure of 10 mTorr, flow rate of 10 standard cubic centimeters per minute (sccm) was used for the deposition of buffer layer.

The buffer layer decreases the lattice mismatch between the sapphire and ZnO films. The substrates were then cooled down to a temperature of 300 ^{O}C or held at the same temperature of 700 ^{O}C. p-type and n-type films of 1 μm thick were grown on the substrates by sputtering the high-purity ceramic ZnO and dopants targets (Zn_3As_2, Zn_3P_2,

ZnO/P_2O_5, Li_3PO_4, Al and ZnO/Al (2% by weight) with an RF power of 100 W for a set deposition time. Delta and uniform doping techniques have been used to dope the ZnO films with the dopant atoms. Ar or Ar/O_2 (1:1) gas at flow rate of 10 sccm and 10 mTorr pressure have been used for depositing the p-type and n-type films.

In delta doping method the deposition of ZnO on sapphire was continuous and dopant atoms deposition was blocked at periodical intervals with the help of a shutter whereas in uniform doping the deposition of ZnO and dopant atoms was continuous for a given deposition time.

4.2 Experiments conducted for p-type ZnO films through monodoping and results

The lists of experiments in Table 3 were done to dope ZnO with a single dopant comprising P or As. All the experiments were done using the (1:1) mixture of Ar and O_2 as sputtering gas and ZnO target has been used as host semiconductor. The gas flow rate, chamber pressure and substrate temperature were kept at constant values of 10 sccm, 10-mTorr and 300 ^{O}C**.** ZnO/P_2O_5 and Zn_3P_2 ceramic targets were used as source for the P acceptor. Zn_3As_2 target has been used to dope ZnO with As. The RF power used for sputtering the targets was 100 W. The total deposition time in delta doping is calculated by multiplying number of cycles with (shutter on-time + shutter off-time).

As-deposited p-type ZnO films are too resistive to allow Hall effect measurements, hence all the films were annealed in O_2 and N_2 gas at 900 ^{O}C for 3 min to activate the dopant atoms. The average Hall measurement results (shown in Table 4) of these films showed stable *n-type conductivities* with carrier concentrations in the range of 10^{17}-10^{18} cm^{-3}.

Table 3 Experiments conducted for making of p-type ZnO through monodoping.

Sample	Doping technique	Doping Target	Shutter on-time	Shutter off-time	Number of cycles	Deposition Time
111213	Delta	ZnO/P_2O_5	30 sec	2 min	60	150 min
111513	Uniform	Zn_3P_2	_	_	_	120 min
112013	Delta	Zn_3P_2	30 sec	3 min	40	140 min
112213	Delta	Zn_3As_2	30 sec	3 min	40	140 min
112513	Uniform	Zn_3As_2	_	_	_	120 min

Table 4 Hall results of monodoped p-type ZnO films.

Sample	111213	111513	112013	112213	112513
Carrier concentration (cm^{-3})	2.7 E17	2.82 E18	5.1 E18	2.1 E18	1.86 E18
Mobility (cm^2/v-s)	13	30	50	47	40
Resistivity Ω-cm	1.71 E-2	7.3 E-2	2.3 E-2	6.2 E-2	7.6 E-2

Thus monodoping ZnO with Group-V acceptors (P and As) failed to produce stable p-type conductivity. The main reason for the problem could be the compensation of acceptor atoms (P and As) by the donor related defects such as P_{Zn}, hydrogen impurities, zinc interstitials and oxygen vacancies.

4.3 Experiments performed for p-type ZnO through codoping

In this work, results from sputtered ZnO thin films codoped with Li and P are reported. To the best of my knowledge, there have been no reports about codoping

involving Li and P to this date. The prediction is that the codoping technique will decrease in the formation of donor related defects and increase the formation of Li_{Zn} and P_O acceptors. This results in the production of reliable p-type films. All the p-type codoped ZnO films in Table 5 were deposited from high-purity ceramic targets of ZnO and Li_3PO_4. The sputtering gas (Ar/O_2 (1:1)) flow rate and chamber pressure were kept at constant values of 10 sccm and 10 mTorr. The power supplied for the sputtering of targets was 100 W.

Table 5 Experiments conducted for making of p-type ZnO through codoping.

Sample	Doping technique	Substrate Temperature	Doping Target	Shutter on-time	Shutter off-time	Number of cycles	Deposition time
110613	Delta	300 ^{O}C	Li_3PO_4	2 min	2 min	100	400 min
110813	Delta	700 ^{O}C	Li_3PO_4	30 sec	2 min	60	150 min
120213	Uniform	300 ^{O}C	Li_3PO_4	_	_	_	120 min

4.3.1 Sample structures

The ZnO:Li_3PO_4 films prepared by delta and uniform doping have the structures as shown in Figures 24 and 25. The delta doped samples contain mixed layers of ZnO + Li_3PO_4 and the number of layers is equal to the number of cycles of the Dopant (Li_3PO_4) shutter. The uniform doped sample has only one thick layer (1 µm) of ZnO + Li_3PO_4 instead of many layers as in delta doped samples.

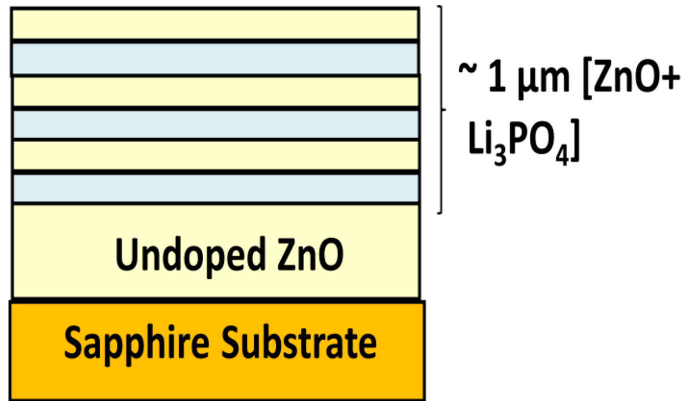

Figure 24 Structure of codoped samples prepared by delta doping.

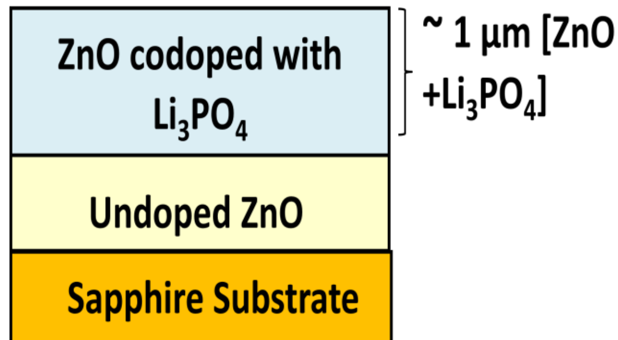

Figure 25 Structure of codoped samples prepared by uniform doping.

4.3.2 Results and analysis

4.3.2.1 Energy-dispersive X-ray spectroscopy (EDX)

It has been used in this work to find out the dopants composition in the as-grown codoped uniform and delta doped ZnO films listed in the Table 5. The Figures 26, 27 and 28 shows the EDX results of these films. The EDX data of delta doped (110813) and uniform doped (120213) films show the presence of phosphorous (P). The weight percent (2.23) of P in 110813 sample is more than the P weight percent (2.09) in sample 120213.

This means that the solubility of P in 110813 sample is higher than in 120213. Due to the detection limit of EDX equipment, it cannot detect the presence of Li in the samples. The EDX result of 110613 sample did not show the presence of P which could be due to its surface inhomogeneity.

Element	Wt%	At%
CK	00.57	01.27
OK	32.21	53.28
ZnL	34.97	14.16
AlK	29.64	29.07
PK	02.60	02.23
Matrix	Correction	ZAF

Figure 26 EDX data of delta doped (110813) sample.

Element	Wt%	At%
CK	08.99	24.06
OK	20.21	40.62
ZnL	70.07	34.46
AlK	00.73	00.87
Matrix	Correction	ZAF

Figure 27 EDX data of delta doped (110613) sample.

Element	Wt%	At%
CK	00.48	01.26
OK	29.33	57.51
AlK	09.46	11.00
PK	02.06	02.09
ZnK	58.66	28.15
Matrix	Correction	ZAF

Figure 28 EDX data of uniform doped (120213) sample.

4.3.2.2 Photoluminescence (PL) Scan

The PL Spectrum of delta doped (110613 and 110813) and uniform doped (120213) films annealed at 700 ^{O}C and 900 ^{O}C for three minutes in O_2 are shown in Figures 29 and 30.

For the samples annealed at 700 ^{O}C, the PL data shows impurity band signals in the energy range of 2.3-2.6 eV which are attributed to the defects such as Zinc and Oxygen vacancies in the films [51]. The small peaks at 3.337 eV are associated with the transition from excitons bound to structural defects [52].

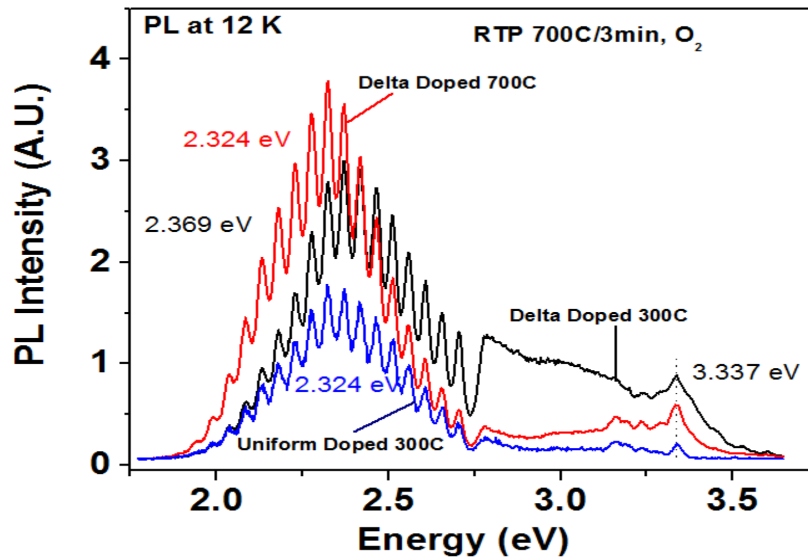

Figure 29 PL data of delta and uniform doped samples annealed at 700 ^{O}C in O_2.

Annealing the samples at 900 ^{O}C in O_2 reduced the intensity of impurity band signals and intensity of other small peaks improved significantly with a shift in the peak values from 3.337eV. This implies that the defects in the samples are minimized and films quality improved considerably.

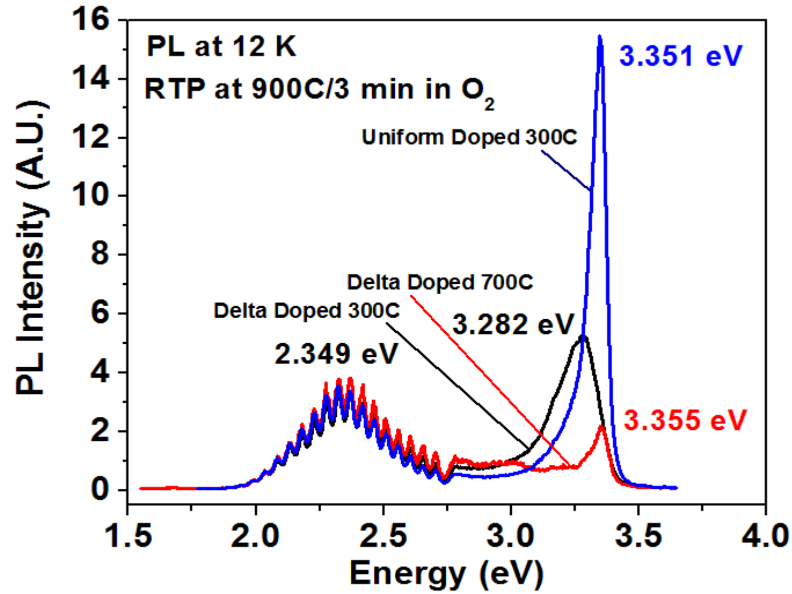

Figure 30 PL data of delta and uniform doped samples annealed at 900 ^{O}C in O_2.

The peaks at 3.351eV and 3.35eV are related to acceptor bound exciton transition $A^{O}X$ transition [53] and the peak at 3.282eV is due to the longitudinal-optical phonon replicas [52]. In this study it is observed that 900 ^{O}C is the best annealing temperature to obtain good quality ZnO: Li_3PO_4 films with minimum defects.

4.3.2.3 X-ray spectroscopy scan (XRD)

The XRD technique has been used to determine the crystal quality of the samples (110613, 110813 and 120213) before and after annealing at 900 ^{O}C for three minutes in O_2. The scan results of these samples are shown in Figure 31. The peaks of the un-annealed films 110813 (delta doped at 700C) and 120213 (uniform doped at 300C) are less intensive and are positioned at angles 34.16° and 34.2° respectively. The un-annealed 110613 (delta doped at 300C) sample did not show any peak. All these indicate the existence of residual compressive stress in the samples which is significantly reduced by the rapid thermal annealing process at 900 ^{O}C.

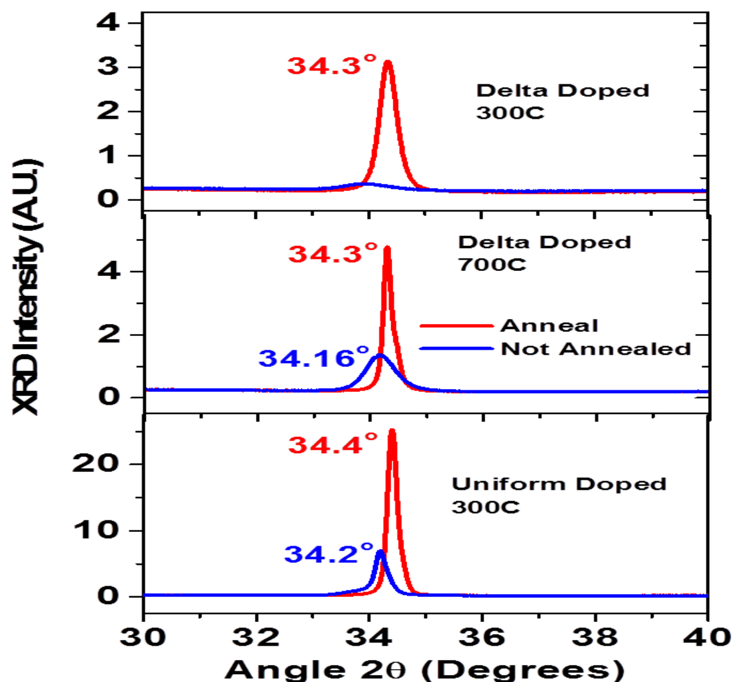

Figure 31 XRD scan of annealed and un-annealed delta and uniform doped ZnO films.

After annealing, the peak intensities of the films improved appreciably and their positions came close to an angle 34.4° (angular position of pure ZnO powder). This implies the crystal quality of the films have improved significantly.

4.3.2.4 Hall effect measurements

Repeated Hall effect measurements were carried out on the annealed (900 ^{O}C) uniform and delta doped films (120213, 110613 and 110813). The Hall results of these films are displayed in Figures 32, 33 and 34, all of them exhibited p-type conductivities. The Hall measurements were repeated for 15 times in light environment. It is noticed that the conductivity of the samples switched randomly between p-type and n-type, the mobility, resistivity and carrier concentration (n) also varied. Similar results were obtained from the Hall measurement test when done in dark environment on the films. The scatter in the results, as well as the inconsistencies in the carrier type, is attributed to

the small hall voltages in the measurements, which can be significantly impacted by small signal noise spikes during the measurements [53]. The average p-type conductivity in the films was determined by averaging the data points of their p-type carrier concentration values. The Table 6 shows the average p-type concentration of the films.

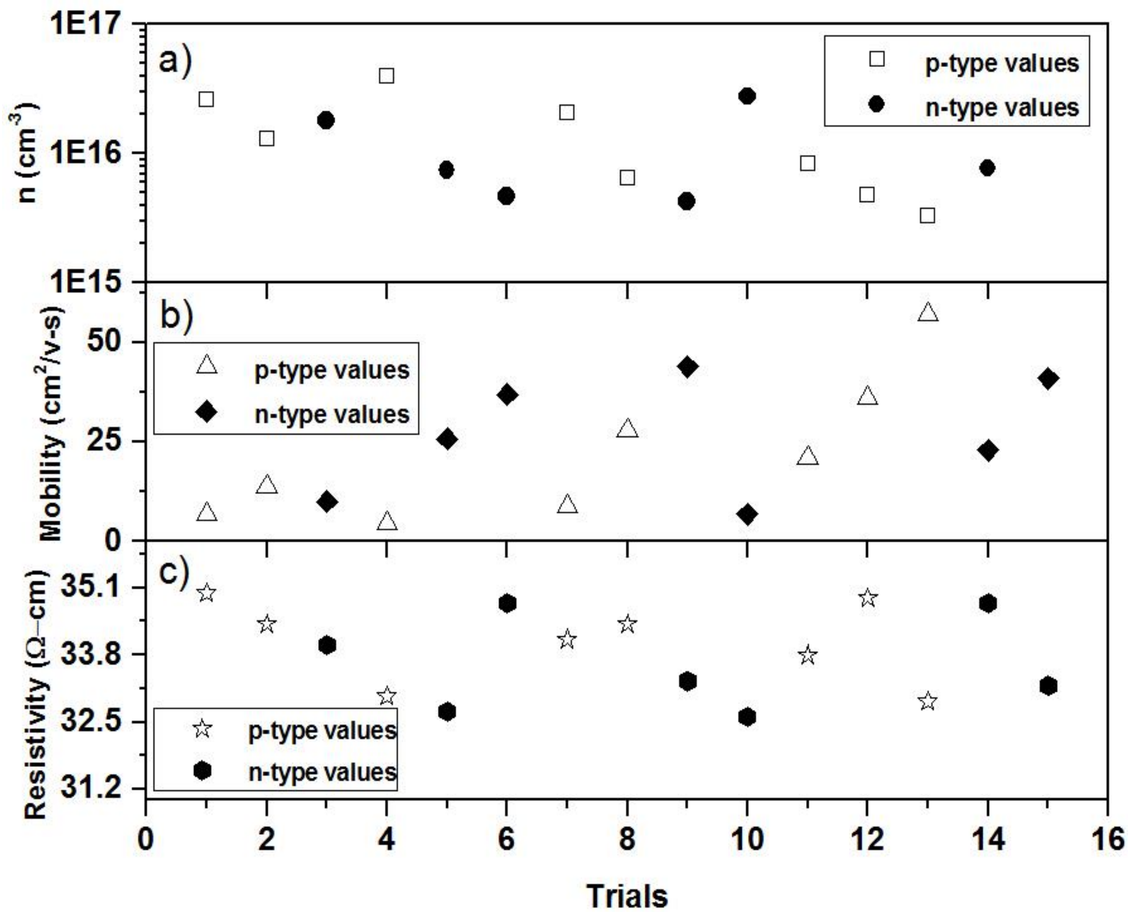

Figure 32 Repeated Hall-effect measurements on the delta doped (110613) sample showing the variation of a) Carrier concentration b) Mobility and c) Resistivity.

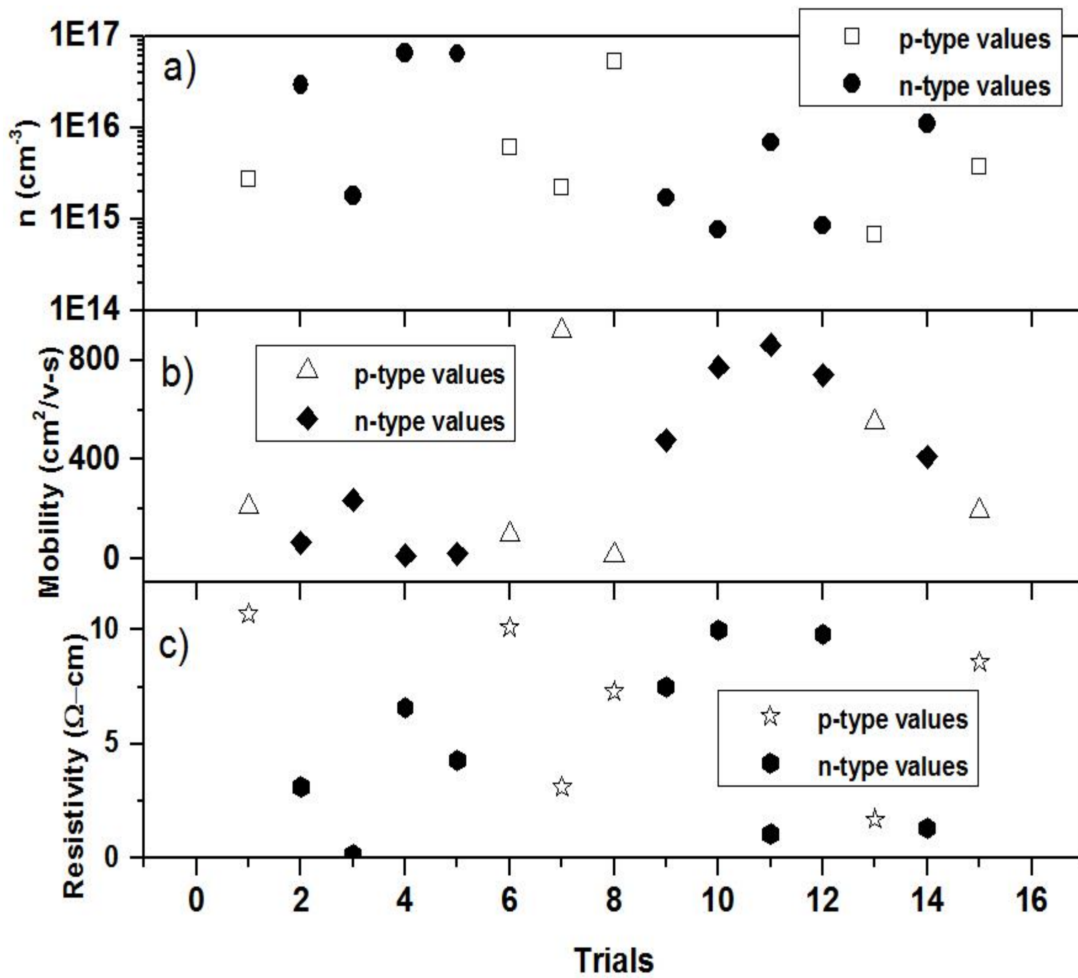

Figure 33 Repeated Hall-effect measurements on the delta-doped (110813) sample showing the variation of a) Carrier concentration b) Mobility and c) Resistivity.

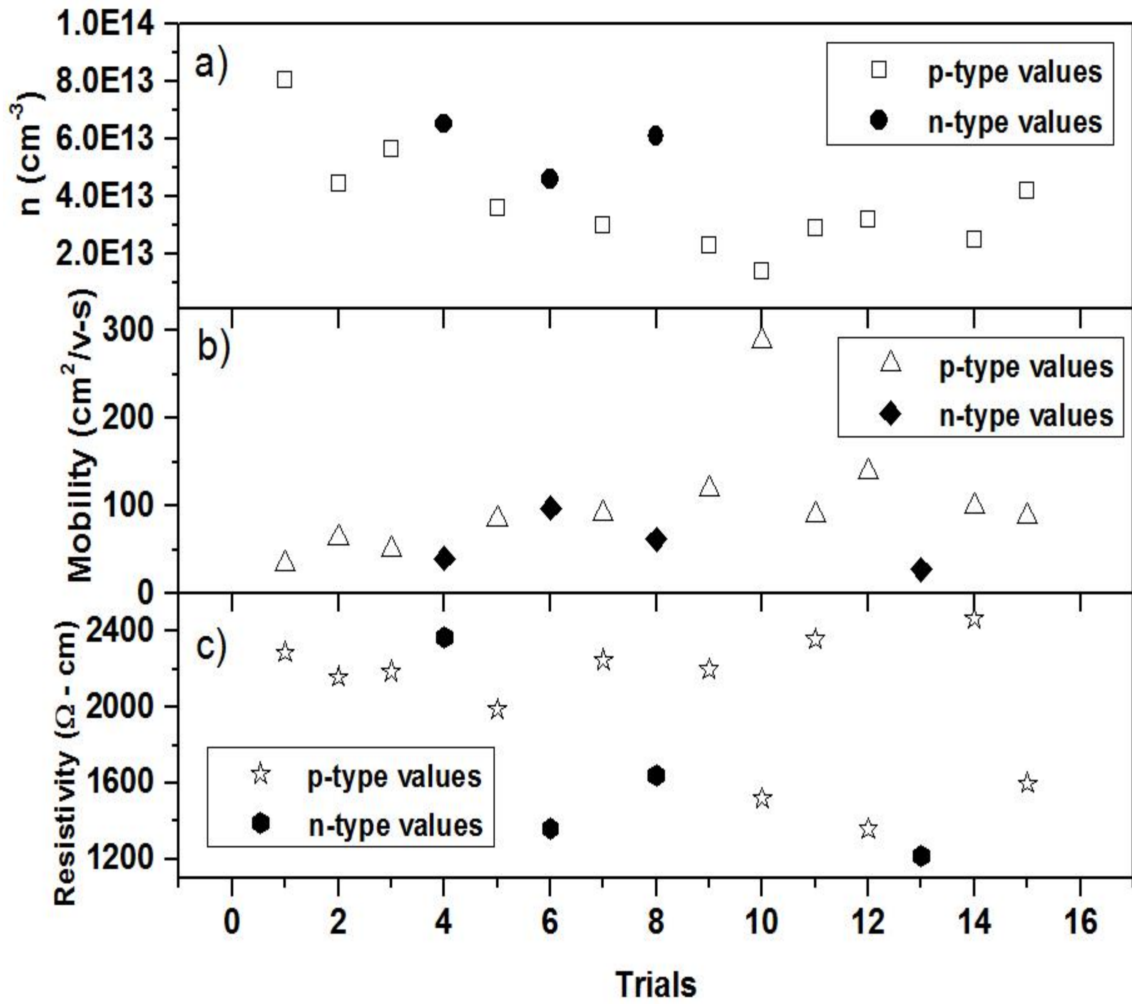

Figure 34 Repeated Hall-effect measurements on the uniform-doped (120213) sample showing the variation of a) Carrier concentration b) Mobility and c) Resistivity.

Table 6 Average p-type concentration of delta and uniform doped samples annealed at 900 ^{O}C in O_2.

Sample	110613 (Delta doped)	110813 (Delta doped)	120213 (Uniform doped)
Hole-concentration (cm^{-3})	1.53×10^{16}	1.13×10^{16}	3.76×10^{13}

The average p-type concentration (1.33×10^{16} cm^{-3}) in the delta doped samples is more than in uniform doped sample (3.76×10^{13} cm^{-3}), which means that the delta doping technique has enhanced the p-type conduction in the samples compared to the uniform doping technique.

4.4 Second set of Experiments conducted for p-type ZnO through codoping

The Table 7 shows the second set of experiments conducted for the codoped p-type films using the delta doping technique. All the samples were annealed in O_2 at 900-^{O}C for 3 min. The Hall measurement test on the samples 091214, 091614 and 092614 did not show any conductivity whereas samples 120413 and 103014 showed conductivity variation between p-type and n-type with an average hole concentration of 2×10^{14} cm^{-3}.

Table 7 Second set of experiments conducted for making of p-type ZnO films.

Sample	Substrate Temp	Doping Target	Shutter on-time	Shutter off-time	Number of cycles	Deposition-time
120413	300 ^{O}C	Li_3PO_4	30 sec	3 min	40	140 min
091214	700 ^{O}C	Li_3PO_4	2 min	2 min	3	12 min
091614	700 ^{O}C	Li_3PO_4	2 min	2 min	1	4 min
092614	700 ^{O}C	Li_3PO_4	2 min	1 min	10	30 min
103014	300 ^{O}C	ZnO/P_2O_5	2 min	10 min	10	120 min

4.5 Experiments conducted for n-type ZnO through monodoping

The Table 8 shows the set of experiments conducted for n-type ZnO films. Al was used as the dopant atom.

Table 8 List of experiments conducted for n-type ZnO.

Sample	Doping technique	Process Gas	Shutter on-time	Shutter off-time	Number of cycles	Total deposition time
100614	Delta	Ar	1 min	5 min	20	120 min
121214	Uniform	Ar/O_2 (1:1)	_	_	_	120 min
121814	Uniform	Ar	_	_	_	120 min
011415	Delta	Ar	1 min	1 min	30	60 min
021315	Delta	Ar	1 min	1 min	60	120 min
032215	Delta	Ar/O_2 (1:1)	1 min	6 min	20	140 min

All the Al doped n-type ZnO samples (1-µm thick) were prepared on double polished sapphire substrates by sputtering the ZnO and Al targets using delta doping method, ZnO/Al (2% by weight) target using uniform doping technique. For all the experiments the substrate temperature was held at 300 ^{O}C, process gas flow rate and chamber pressure were kept at constant values of 10 sccm and 10 mTorr.

4.6 Results and analysis

4.6.1 Hall results of as-grown n-type ZnO films

The Figures 35 and 36 present the repeated Hall measurements of as-grown delta and uniform doped n-type ZnO films (100614 and 121214). The Hall results were found to be stable and consistent in light and dark environments. The electrical properties of as-grown delta (100614) and uniform (121214) doped films providing average electron concentration, mobility and resistivities (calculated from Figures 35 and 36) are tabulated in Table 9. It was observed that the electron concentration and mobility in the sample 100614 was improved by an order of magnitude as compared to sample 121214, while the resistivity was found reduced by two orders of magnitude. These measurements strongly imply that as-grown delta doped sample was highly n-type conductive than the uniform doped sample. The Hall measurement test on rest of the as-grown samples (121814, 011415, 021315 and 032215) did not show any conductivity.

Table 9 Electrical properties of specific as-grown n-type films.

Sample	Delta doped sample (100614)	Uniform doped sample (121214)
Electron concentration (cm^{-3})	2.79 E19	1.82 E18
Mobility (cm^2/v-s)	1.58 E1	3.6 E-1
Resistivity (Ω-cm)	1.432 E-2	9.3

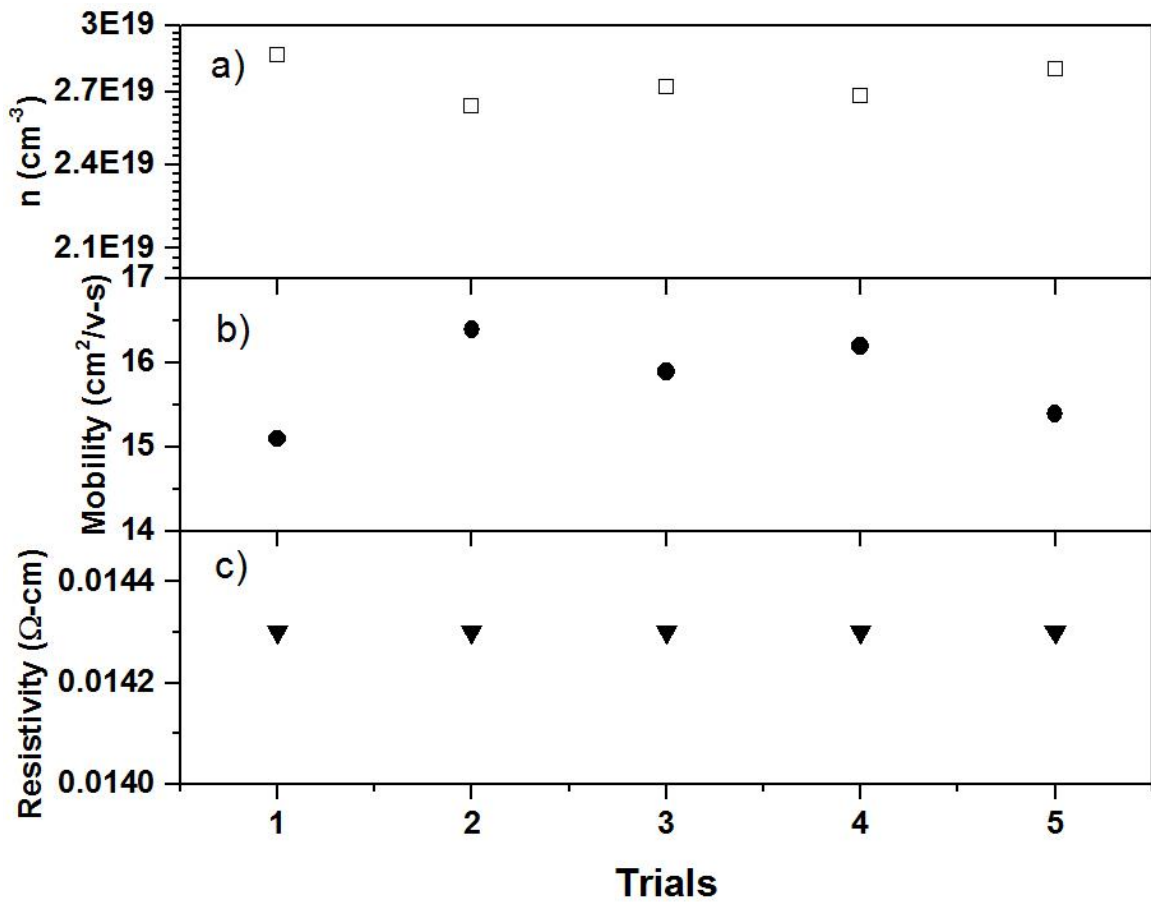

Figure 35 Repeated Hall-effect measurements on the as-grown delta-doped (100614) sample showing a) Carrier concentration b) Mobility and c) Resistivity.

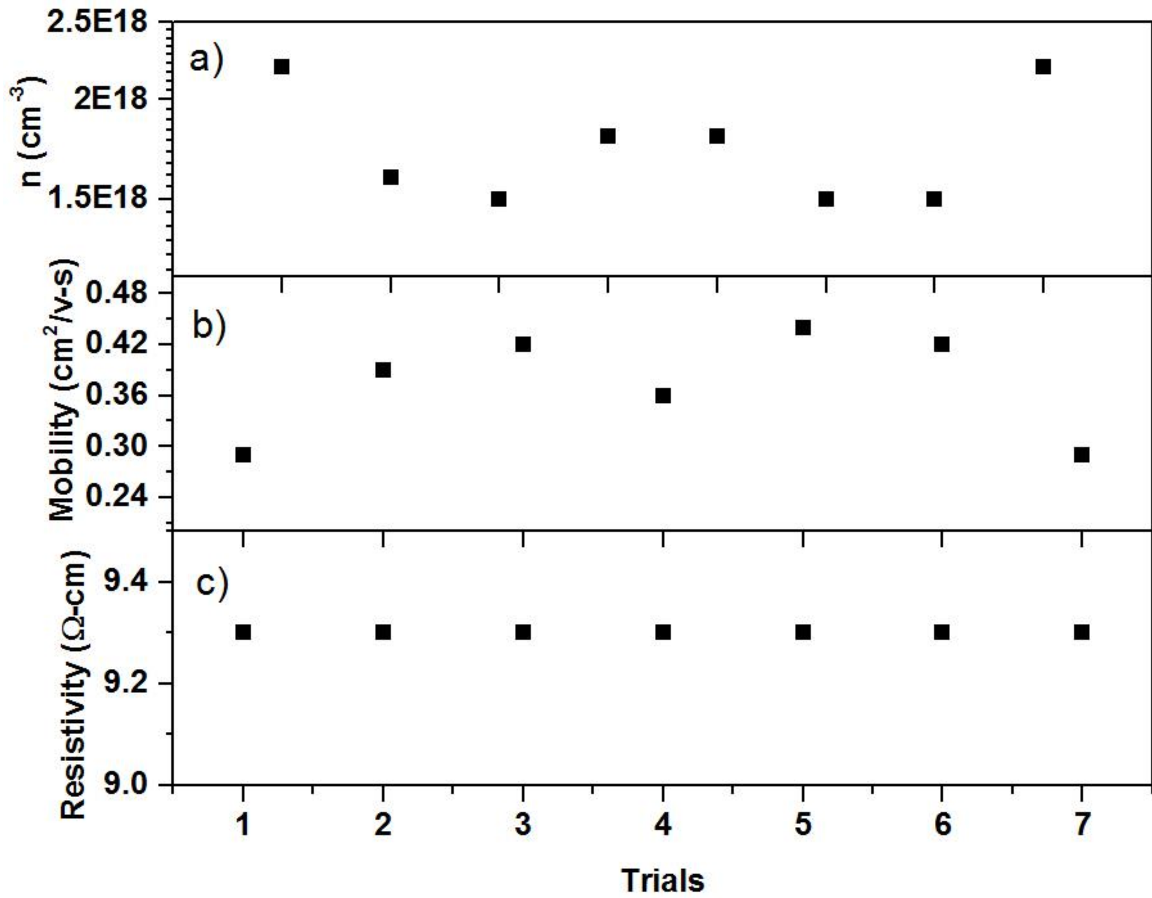

Figure 36 Repeated Hall-effect measurements on the as-grown uniform-doped (121214) sample showing a) Carrier concentration b) Mobility and c) Resistivity.

4.6.2 Hall results of N_2 and ($N_2 + O_2$) annealed n-type ZnO films

All the n-type ZnO films listed in Table 8 were annealed in N_2 at 900 ^{O}C for 3 minutes. Table 10 displays the electrical properties of 032215 and 121214 samples obtained from their repeated Hall measurements.

Table 10 Electrical properties of specific N_2 annealed n-type films

Sample	Delta doped film (032215)	Uniform doped film (121814)
Electron concentration (cm^{-3})	1.2 E19	3 E19
Mobility (cm^2/v-s)	3.4	3.75
Resistivity (Ω-cm)	1.6 E-2	5.7 E-2

The electrical properties of these samples indicate that the uniform doped sample (121814) is slightly more n-type conductive than the delta doped sample (032215). The Hall test on the remaining (N_2) annealed samples (100614, 121814, 011415 and 021315) did not show any conductivity.

All the n-type ZnO films were also annealed in O_2 at 700 ^{O}C for 2 min followed by annealing in N_2 at 900 ^{O}C for 3 minutes. Table 11 represents the electrical properties of these films. Apart from 032215, rest of the delta doped samples (100614, 011415 and 021315) exhibited carrier concentrations in the order of 10^{18} cm^{-3}. The film 032215 showed a carrier concentration in the order of 10^{19} cm^{-3}. It was noticed that all the delta doped films were less n-type conductive than uniform doped ones (121214 and 121814),

which exhibited highest carrier concentrations of 5 E19 cm^{-3} and 1.1 E20 cm^{-3}. The electrical properties of these samples were found to be stable in both the environments (light and dark)

Table 11 Electrical properties of N_2 + O_2 annealed films.

Sample	100614 (Delta-Doped)	121214 (Uniform-doped)	121814 (Uniform-doped)	011415 (Delta-Doped)	021315 (Delta-Doped)	032215 (Delta-Doped)
Carrier concentration (cm^{-3})	3.7 E18	1.1 E20	5 E19	1.7 E18	1.2 E18	1.6 E19
Mobility (cm^2/v-s)	16	15	7	26	3	1.3
Resistivity Ω-cm	1 E-1	4.5 E-3	2.08 E-2	1.3 E-1	1.8	2.8 E-1

4.6.3 XRD scan

The Figures 37 and 38 show the x-ray scan results of annealed (N_2+ O_2), as-grown delta and uniform doped n-type ZnO films (032215 and 121214). The peaks amplitudes of the as-grown films increased after annealing which means that the crystal quality of these films is improved. The sharp peaks in all the cases were close to 34.4° (angular position of pure ZnO powder). This implies that all the films have preferential orientation along the c-axis (001).

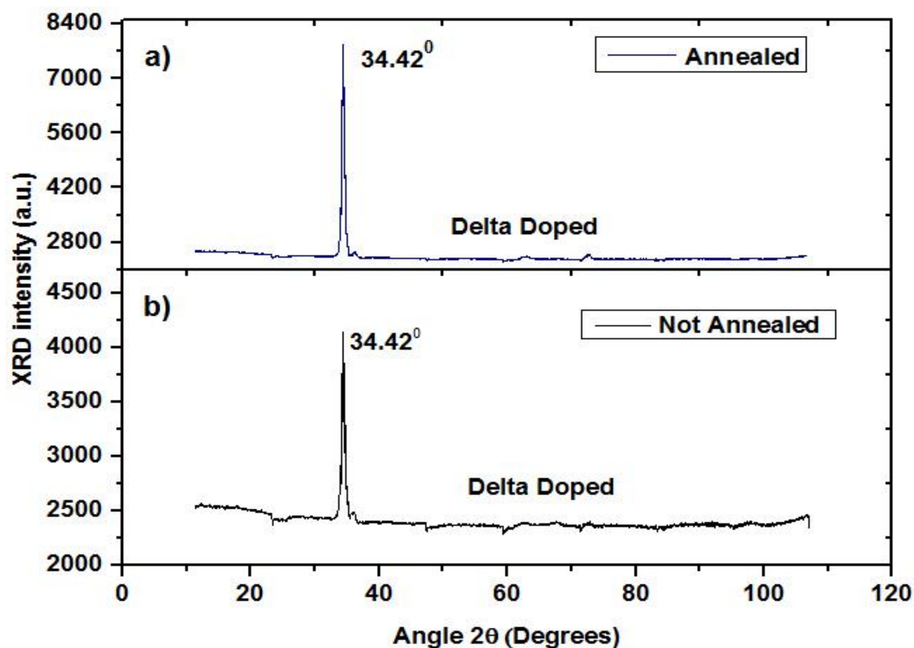

Figure 37 XRD scan of annealed (N_2+ O_2) and un-annealed delta doped sample (032215).

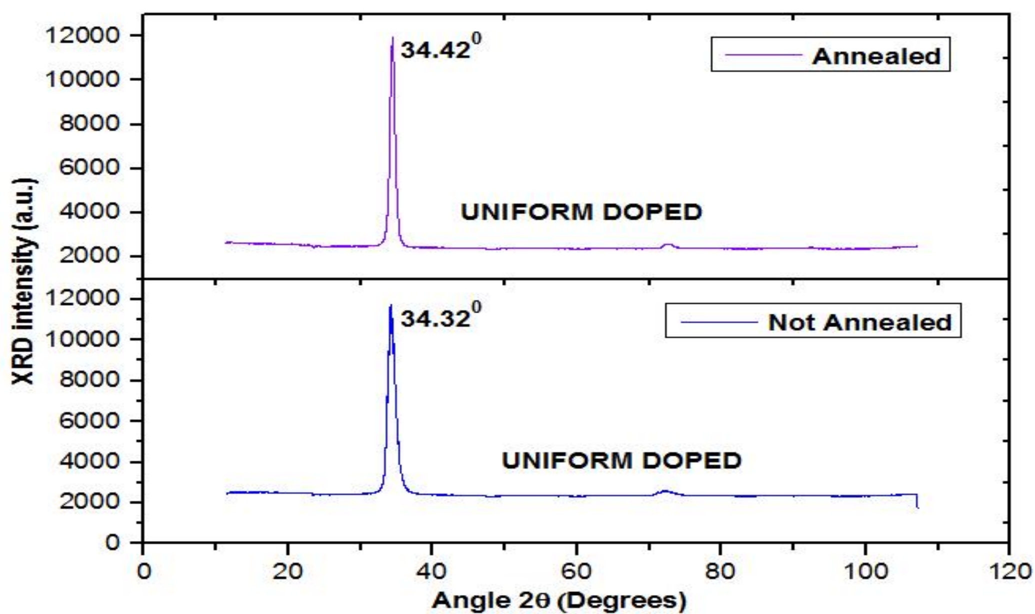

Figure 38 XRD scan of annealed (N_2+ O_2) and un-annealed uniform doped sample (121214).

4.6.4 PL scan

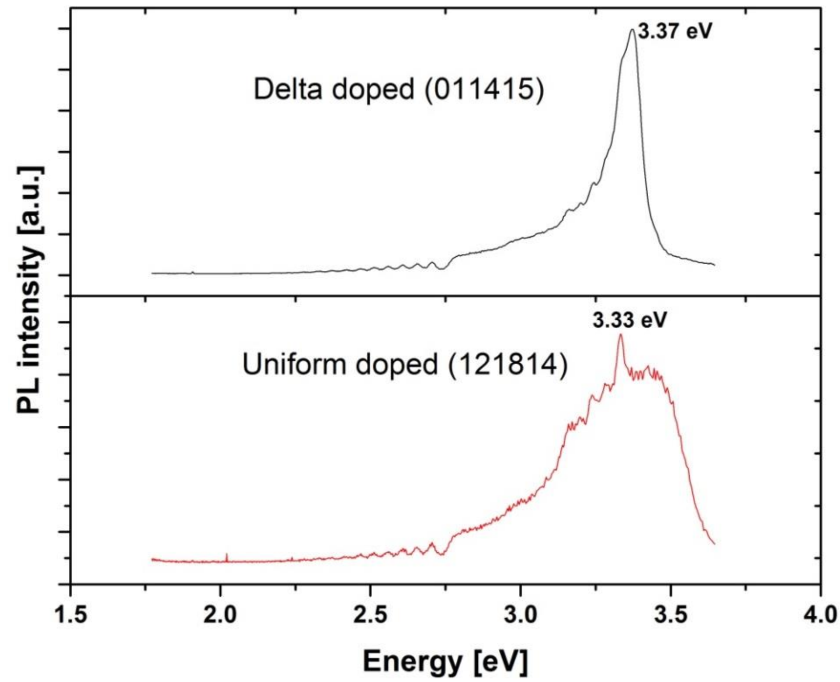

Figure 39 PL data of delta and uniform doped samples annealed in ($N_2 + O_2$).

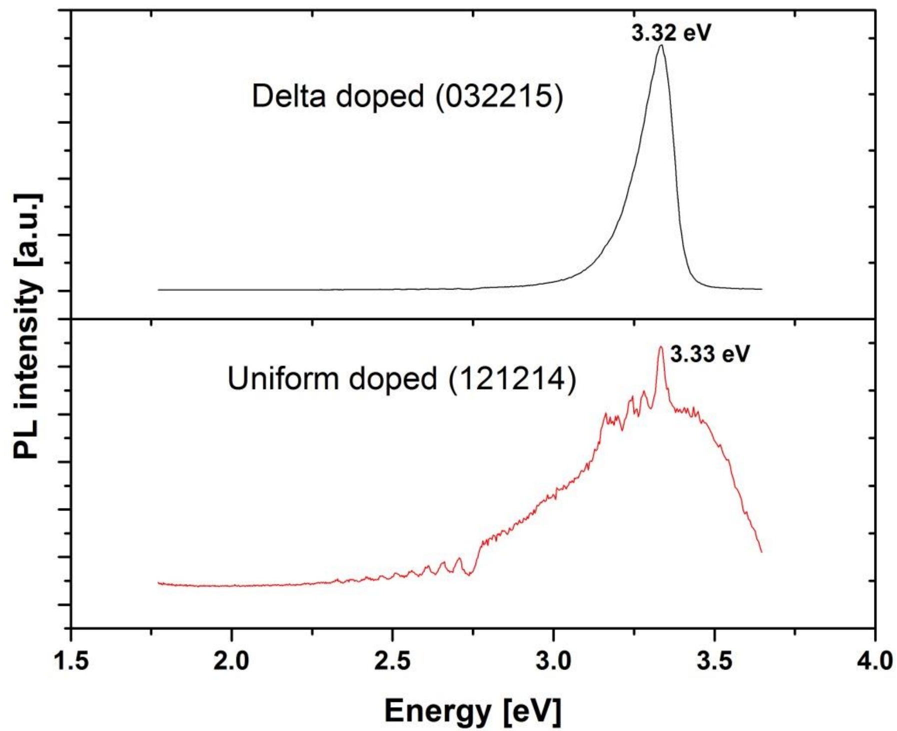

Figure 40 PL data of Second set delta and uniform doped samples annealed in ($N_2 + O_2$).

The Figures 39 and 40 display the PL scan results of annealed (N_2 + O_2) delta (011415 and 032215) and uniform doped samples (121814 and 121214). The PL intensity of the peaks of delta doped films are very sharp then the uniform doped films. This means that the uniform doped films contain more defects over the delta doped films.

Chapter 5

Conclusion

5.1 Conclusion

p-type and n-type ZnO films were fabricated on sapphire substrates using uniform and delta doping techniques through RF magnetron sputtering at substrate temperatures of 300 ^{O}C and 700 ^{O}C. The gases used to sputter the ZnO and dopant targets were Ar/O_2 (1:1) mixture or Ar. Monodoping ZnO with P and As produced n-type conductivities. The codoped (Li + P) p-type films were annealed in O_2 at 900 ^{O}C for 3 minutes, n-type films were annealed in N_2 and O_2 at 700-900 ^{O}C for 3-5 minutes to improve the films electrical properties. XRD data showed the decrease of residual stress on the p-type films after annealing. Hall measurement test on the annealed (900 ^{O}C) delta doped p-type films (110613 and 110813) revealed average Hall concentration of 1.33 x 10^{16} cm^{-3}, while uniform doped p-type film (120213) produced an average carrier concentration of 3.76 x 10^{13} cm^{-3} which implied that delta doped films are more p-type conductive than the uniform doped film. The PL scan results of the films 110813 and 120213 showed emission peaks at 3.35 eV which are attributed to $A^{O}X$ transitions. The EDX results showed the presence of acceptor P in these films.

The as-grown n-type delta doped sample (100614) exhibited good electrical properties with an average electron concentration of 2.79 E19 cm^{-3} and resistivity of 0.014 Ω-cm as compared to uniform doped sample (121214) which showed an average carrier concentration of 1.82 E18 cm^{-3} and resistivity of 9.3 Ω-cm. The uniform doped n-type films annealed in N_2 and (O_2+N_2) exhibited average carrier concentrations in the order of 10^{19}-10^{20} cm^{-3} and are better n-type semiconductors over the annealed delta

doped ones, which showed carrier concentration in the order of 10^{18}-10^{19} cm^{-3}. The enhancement in the electrical conductivity of the samples was more with (N_2 + O_2) annealing than N_2 annealing. The XRD scan results on n-type delta (032215) and uniform doped (121214) films indicated that these films have preferred orientation along the C-axis (001) plane and the crystal quality of the films were improved after annealing. The PL scan data of specific n-type ZnO films showed the presence of more defects in uniform doped samples compared to delta doped ones.

5.2 Future work

It was reported in literature [23] that codoping ZnO with donor and acceptor impurities could increase the acceptor solubility and decrease the acceptor binding energy. Nitrogen is most promising one among the Group V elements to dope ZnO p-type, but the issue with nitrogen doping is its low solubility in ZnO. Al could be used to increase the nitrogen solubility. The future work could be trying to dope ZnO with Al and N at different experimental conditions to achieve highly stable and conductive p-type material. The annealing temperatures used for n-type films could be still optimized to get the best n-type conductivity.

References

1. Chennupati Jagadish and Stephen J. Pearton, "*Zinc Oxide Thin Films and Nanostructures Processing Properties and Applications*," Elsevier, Netherlands, 2006.

2. Zhe Chuan Feng, "*Handbook of Zinc Oxide and Related Materials*," CRC press, Florida, 2013.

3. Claus Franz Klingshrin, Bruno K. Meyer, Andreas Wagg, Axel Hoffman and Jean Geurts, "*Zinc oxide From Fundamental Properties Towards Novel Applications*," Springer Series in Material Science, Berlin, 2010

4. Sidra Sabir, Muhammad Arshad and Sunbal Khalil Chaudhari, "*ZnO Nanoparticles for Revolutionizing Agriculture: Synthesis and Applications,"* The Scientific World Journal, Vol.2014, pp. 1-8, Nov 2014.

5. Manish Kumar and Shakthi Swarup Sahu, *"ZnO Nanostructures Synthesized by Oxidation of Zinc,"* Bachelor of technology thesis, National institute of technology, Rourkela, 2010.

6. Anderson Janotti and Chris G. Van de Walle "*Native point defects in ZnO*," Phys.Rev.B, Vol.76, pp. 165202, Oct 2007.

7. Anderson Janotti & Chris G. Van de Walle "*Hydrogen multicenter bonds*," Nature- Materials, vol.6, pp. 44-47, Dec 2006.

8. Hadis Morkoç and Ümit Özgür, *"Zinc Oxide: Fundamentals, Materials and Device Technology,"* Wiley-VCH, Germany, 2009.

9. K.S.Shtereva, V.Tvarozek, M.Netrvalora, P.Sutta and A.Pullmannova, "*Effect of Doping on the Optical and Structural properties of ZnO Thin Films Prepared by RF Diode Sputtering,*" Ecs Transactions, vol.25, no.12, pp. 65-72, 2009.

10. P.A.Rodnyi and I.V.Khodyuk, "*Optical and Luminescence Properties of Zinc Oxide*," Sprinker link, vol.111, no.5, pp. 814-824, Dec 2011.

11. Pallab Bhattacharya, Roberto Fornari and Hiroshi Kamimura, *"Comprehensive Semiconductor Science and Technology,"* Elsevier, Italy, 2011.

12. D.P. Norton, Y.W. Heo, M.P. Ivill, K. Ip, S.J. Pearton, M.F. Chisholm and T. Steiner, "*ZnO: growth, doping & processing*," Materials today, vol.7, no.7, pp. 34-40, May 2004.

13. Cole W. Litton, Donald C. Reynolds and Thomas C. Collins, "*Zinc Oxide Material for Electronic and Optoelectronic Device Applications*," Wiley, United Kingdom, 2011.

14. Ümit Özgür, "ZnO Devices and Applications: *A Review of Current Status and Future Prospects*," Proceedings of the IEEE, vol.98, pp. 1225-1268, 2010.

15. Jim Lee, "*Microstructure and Properties of Zinc Oxide Nano-Crystalline Thin Films and Composites*," Phd dissertation, University of Auckland, New Zealand, 2006.

16. L.Lyons, A.Janotti and C.G. Van de Walle, "*Why nitrogen cannot lead to p-type conductivity in ZnO,"* Appl.Phys.Lett, vol.95, pp. 252105, Dec 2009.

17. M.D.Mccluskey and S.J.Jokela, "*Defects in ZnO*," Phys.Rev.B, vol.76, no.7, pp. 165202, Oct 2007.

18. EC.Lee, Y.S.Kim, Y.G.Jin and K.J.Chang, *"Compensation mechanism for N acceptors in ZnO,"* Phys.Rev.B, vol.64, pp. 85120, Aug 2001.

19. W. J. Lee, J. Kang, *and* K. J. Chang, *"Defect Properties and p-Type Doping Efficiency in Phosphorus-Doped ZnO,"* Phys. Rev. B, vol.73, pp. 024117, Jan 2006.

20. J.C.Fan, K.M.Sreekanth, Z.Xie, S.L. Chang, K.V.Rao,"*P-type ZnO materials: Theory, growth, properties and devices*," progress in material science, Vol.58, issue-6, PP 874-985, March 2013.

21. S.Limpijumnong, S.B.Zhang, S.H.Wei and C.H.Park, "*Doping by Large-Size-Mismatched Impurities: The Microscopic Origin of Arsenic- or Antimony-Doped p-Type Zinc Oxide,*" Phys.Rev.Lett, vol.92, no.15, pp. 15501, Apr 2004.

22. Park CH, Zhang SB and Wei S-H, "*Origin of p-type doping difficulty in ZnO: The impurity perspective,"* Phys.Rev.B, vol.66, pp. 073202, Aug 2002.

23. T.Yamamoto, "*Codoping Method for Solutions of Doping Problems in Wide-Band-Gap Semiconductors*," Physics status solid, vol.193, pp. 423-433, Jun 2002.

24. R.Y.Tian and Y.J. Zhao, "*The origin of p-type conduction in (P, N) codoped ZnO,*" J.Appl.Phys, vol.106, pp. 043707, Aug 2009.

25. J.G. Lu, Y.Z. Zhang, Z.Z. Ye, L.P. Zhu, L. Wang, B.H. Zhao and Q.L. Liang, "*Low-resistivity, stable p -type ZnO thin films realized using a Li–N dual-acceptor doping method,*" App.Phys.Lett, vol.88, pp. 222114, Jun 2006.

26. E.F.Schubert, "*Delta doping of Semiconductors,"* Cambridge University Press, Cambridge, 1996.

27. J.J.Harris, "*Delta-doping of semiconductors*," springer link, vol.4, no.2, pp. 93-105, Jun 1993.

28. C.E.C. Wood*,* G.M. Metze*,* J.D. Berry, and L.F. Eastman, "*Complex Free-Carrier Profile Synthesis by 'atomic-plane' Doping of MBE,"* J. Appl. Phys., vol.51, pp.383-387, 1980.

29. E. F. Schubert and K. Ploog, "*The δ-Doped Field-Effect Transistor*," Jpn. J. Appl. Phys, vol.24, no.8, pp.L608-L610, July 1985.

30. M.L.Nakarmi, K.H.Kim, J.Li, J.Y.Lin and H.X.Jiang, "*Enhanced p-type conduction in GaN and AlGaN by Mg-doping,"* App.Phys.Lett, vol.82, pp. 3041-3043, Jan 2003.

31. C.Bayaram, J.L.Pau, R.McClintock and M.Razeghi, "*Delta-doping optimization for high quality p-type GaN,"* J.Appl.phys, vol.104, pp. 083512, Oct 2008.

32. O. Contreras, F.A. Ponce, J. Christen, A. Dadgar, and A. Krost, "*Dislocation annihilation by silicon delta-doping in GaN epitaxy on Si*," Appl. Phys. Lett., vol. 81, pp. 4712–4714, 2002.

33. Yingda chen, Hualong Wu, Guanglong Yue, Zimin Chen, Zhiyuan Zheng, Zhisheng Wu, Gang Wang and Hao Jiang, "*Enhanced Mg Doping Efficiency in P-Type GaN by Indium-Surfactant-Assisted Delta Doping Method*," Appl.Phys.exp, vol.6, no.4, pp. 041001, Mar 2013.

34. H.D. Jung, C.D. Song, S.Q. Wang, K. Arai, Y.H. Wu, Z. Zhu, T.Yao and H. Katamaya-Yoshida, "*Carrier concentration enhancement of p-type ZnSe and ZnS by codoping with active nitrogen and tellurium by using a δ-doping technique,"* Appl.Phy.Lett, vol.70, pp.1143-1145, 1997.

35. W.Lin, S.P.Guo, M.C. Tamargo, I. Kuskovsky, C.Tian and G.F. Neumark, "*Enhancement of p-type doping of ZnSe using a modified (N+Te) δ-doping technique*," Appl.Phy.Lett, vol.76, no.16, pp. 2205-2207, Apr 2000.

36. Stephen M Rossnagel, "*Hand book of thin film deposition process and techniques*," Noyes publications, USA, 2001.

37. Madhavi Oleti Kalki Rajan, "*Characterization of P-type ZnO films,*" Master thesis, University of South Florida, Florida, 2004.

38. Available: http://www.directvacuum.com/sputter.asp, [retrieved 9 Mar 2015].

39. Bo Cui, "Thin film deposition III," Available: https://ece.uwaterloo.ca/~bcui/?page_id=20, [retrieved 7 Mar 2015].

40. Available: http://www2.difest.unipr.it/thifilab/ImmaginiThiFiLab/Sputtering.html, [retrieved 7 Jul 2015].

41. A.K.Chattopadhay, "Technology of surface coating," Available: http://nptel.ac.in/courses/112105053/14, [retrieved 8 Mar 2015].

42. Erli Chen, "Thin film deposition-II," Available: http://www.mrsec.harvard.edu/education/ap298r2004/Erli%20chenFabrication%20II%20-%20Deposition-1.pdf, [retrieved 5 Mar 2015].

43. *"*Sputtering (cont.) and Other Plasma Process*,"* Available: http://users.wfu.edu/ucerkb/Nan242/L08-Sputtering_b.pdf, [retrieved 8 Mar 2015].

44. Available: http://marriott.tistory.com/97, [retrieved 13 Apr 2015].

45. Available:http://www.lesker.com/newweb/deposition_materials/depositionmaterials_sputtertargets_1.cfm?pgid=zn2, [retrieved 7 Jul 2015].

46. Ayse Seyhan, "*Photoluminescence spectroscopy of CdS and GaSe,"* Master thesis, Middle East Technical University, Sep 2003.

47. Peter Y.Yu and Manuel Cardona, "*Fundamentals of semiconductors*," springer, Newyork, USA, 1999.

48. Available:http://chemwiki.ucdavis.edu/Analytical_Chemistry/Analytical_Chemistry_2.0/10_Spectroscopic_Methods/10A%3A_Overview_of_Spectroscopy, [retrieved 6 Apr 2015].

49. Available: http://magufos.com/13448/el-efecto-hall, [retrieved 15 Mar 2015].

50. W.Robert Thurber, "Hall Effect Measurement," Available: http://www.nist.gov/pml/div683/hall_intro.cfm, [retrieved 16 Mar 2015].

51. BO Cai, Mim Lal Nakarmi, Tom Nelson Oder, Michael Mcmaster and N.Velpukonda, "*Elevated temperature dependent properties of phosphorous and arsenic doped Zinc oxide thin films*," J.Appl.Phys, vol.114, pp. 223709, Dec 2013.

52. Ü. Özgür, Ya. I. Alivov, C. Liu, A. Teke, M. A. Reshchikov, S. Doğan, V. Avrutin, S.-J. Cho and H. Morkoç,"*A comprehensive review of ZnO materials and devices,"* J.Appl.Phys, vol.98, no.4, pp. 041301, Aug 2005.

53. Tom Nelson Oder, Andrew Smith, Mark Freeman, Michael Mcmaster, BO Cai and Mim Lal Nakarmi, "*Properties of ZnO Thin Films Codoped with Lithium and Phosphorous*," J.Electronic materials, vol.43, pp. 1370-1378, Mar 2014.